The Mesoproterozoic Irumide belt of Zambia

B. De Waele [a,*], A.B. Kampunzu [b], B.S.E. Mapani [c], F. Tembo [d]

[a] Tectonics Special Research Centre, Department of Applied Geology, Curtin University of Technology, G.P.O. Box U1987, Perth, WA 6845, Australia

[b] Geology Department, University of Botswana, Private Bag 0022, Gaborone, Botswana

[c] University of Namibia, Department of Geology, Private Bag 13301, Windhoek, Namibia

[d] Geology Department, School of Mines, University of Zambia, P.O. Box 32379, Lusaka, Zambia

Abstract

The Mesoproterozoic Irumide belt is a northeast-trending structural province stretching from central Zambia to the Zambia–Tanzania border and northern Malawi. Mesoproterozoic and Neoproterozoic transcurrent shear zones within reactivated parts of the Palaeoproterozoic Ubendian belt define its northeastern limit. The northwestern margin is defined by the largely undeformed basement lithologies of the Bangweulu block. An intensely folded and sheared zone at the southeastern margin of the Mporokoso Group sedimentary depocentre on the Bangweulu block, interpreted to have developed above a thrust at the basement-cover interface, indicates that far-field effects of the Irumide Orogen also affected the southeastern part of the Bangweulu block sedimentary cover. To the west and southwest, Irumide and basement lithologies were reworked by the Damara–Lufilian–Zambezi Orogen within the Neoproterozoic Zambezi and Lufilian belts. The Choma–Kalomo block, previously regarded as the southwesterly continuation of the Irumide belt, is a distinct Mesoproterozoic province, while a succession of structurally juxtaposed tectonic terranes in eastern Zambia record a deformation event related to the Irumide Orogen. The lithological units identified in the Irumide belt include: (1) limited Neoarchaean rocks emplaced between 2.73 and 2.61 Ga and representing the oldest rocks in the Bangweulu block; (2) ca. 2.05–1.85 Ga volcano-plutonic complexes and gneisses representing the most important components in the Bangweulu block; (3) an extensive quartzite–metapelite succession with minor carbonate forming the Muva Supergroup, and deposited at ca. 1.85 Ga; (4) granitoids emplaced between 1.65 and 1.55 Ga; (5) a minor suite of anorogenic plutons (nepheline syenite and biotite granite) restricted to the far northeastern Irumide belt and emplaced between 1.36 and 1.33 Ga; (6) voluminous syn- to post-kinematic Irumide granitoids emplaced between 1.05 and 0.95 Ga. Crustal shortening and thickening in the Irumide belt are shown by northwestward-directed thrusts and related folds and metamorphic parageneses recording a clockwise medium-pressure/medium-temperature P–T–t path. Metamorphic grades range from greenschist facies in the foreland to the northwest to upper amphibolite facies in the southeast, with local granulites. Peak metamorphism is diachronous across the belt and bracketed between 1.05 in the southeast and 1.02 Ga in the northwest.

Keywords: Irumide belt; Palaeoproterozoic Muva Supergroup; Mesoproterozoic granitoids; Bangweulu block

1. Introduction

The Irumide belt is a northeast-trending fold and thrust belt (Fig. 1) that stretches from central Zambia, where it is truncated by the Neoproterozoic Zambezi belt, to the Zambia–Tanzania–Malawi border in the northeast, where it terminates against northwest-trending shear zones (Daly, 1986; Theunissen et al., 1996; Klerkx et al., 1998). The Irumide belt was first described by Ackermann (1936, 1950, 1960), Ackermann and Forster (1960) and Forster (1965) who referred to the granitic basement complex in the Irumide belt as "Die Mkushi Gneisse" and the extensive metasedimentary succession of quartzite and metapelite as "Die Muva". To the northwest of the Irumide belt, a

* Corresponding author.
E-mail address: info@bdewaele.be (B. De Waele).

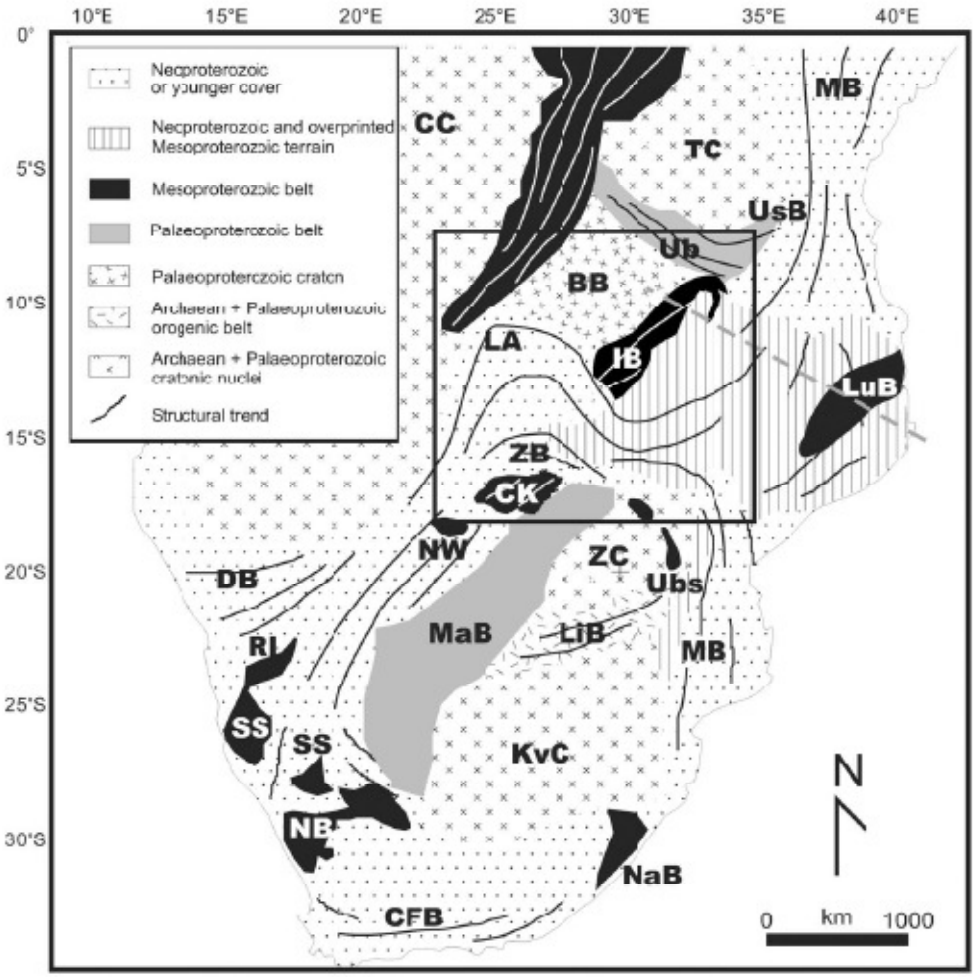

Fig. 1. Tectonic provinces of central and southern Africa. BB = Bangweulu block; CC = Congo Craton; CFB = Cape Fold belt (Saldania belt); CK = Choma–Kalomo block; DB=Damara belt; KB = Kibaran belt; KvC = Kaapvaal Craton; LA = Lufilian belt; LiB = Limpopo belt; LuB = Lurio belt; MaB = Magondi belt; MB = Mozambique belt; NaB = Natal belt; NB = Namaqua belt; NW = northwest Botswana Rift; RI = Rehoboth Inlier; SS = Sinclair Sequence; TC = Tanzania Craton; Ub = Ubendian belt; Ubs = Umkondo basin; UsB = Usagaran belt; ZB = Zambezi belt; ZC = Zimbabwe Craton. Dashed line shows the location of a regional cross-section in Fig. 15.

complex of granites and gneisses was ascribed to the Bangweulu block and presumed to be of Archaean age (Forster, 1965). Daly and Unrug (1982) and Andersen and Unrug (1984) extended the term Muva Supergroup to include the sedimentary rocks of the Mporokoso Group and the Kasama Formation on the Bangweulu block, and the Mitoba River and Manshya River Groups and correlatives in the Irumide belt (Fig. 2). The Manshya River and Kanona Group metasedimentary sequence predominantly consists of shallow marine deposits, whereas fluvial and lacustrine deposits dominate the Mporokoso Group. Previously, the age of sedimentation was poorly constrained between the waning stages of magmatism in the Bangweulu block (ca. 1.82 Ga) and the intrusion of the Luserga syenite (1145 ± 20 Ma, Brewer et al., 1979, Fig. 2, Table 1, no. 48).

The Irumide belt displays overall northwesterly tectonic vergences, placing rocks affected by Irumide deformation on top of undeformed Palaeoproterozoic (~2.05–1.85 Ga) rocks of the Bangweulu block in northern Zambia. Within

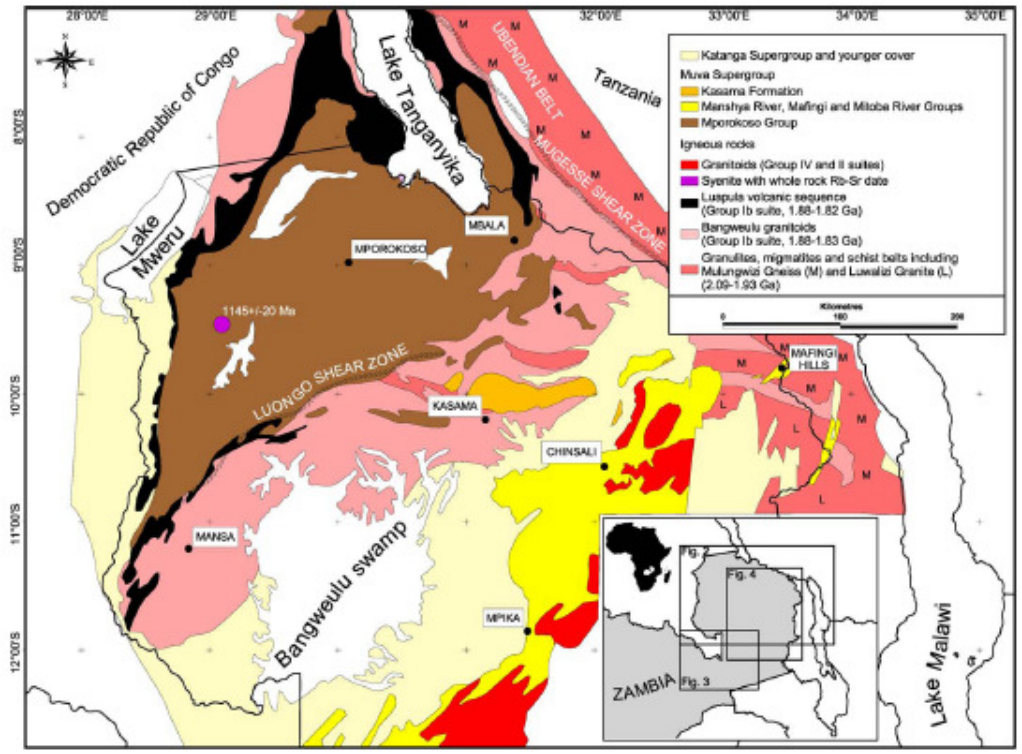

Fig. 2. Geological map of northern Zambia. Assembled and modified after Andersen and Unrug (1984) and Thieme and Johnson (1981).

the Irumide belt, metamorphic grade changes rapidly across strike, and this led earlier workers (Stillman, 1965; Moore, 1967) to subdivide the metasedimentary units into an older high-grade metamorphic sequence and a younger low-grade sequence. De Waele and Mapani (2002) showed that this subdivision of essentially identical stratigraphic sequences, based on differences in metamorphic grade alone, is untenable.

Over the past 10 years a large amount of new data has been acquired in the Irumide belt, shedding new light on this poorly documented structural province. This paper presents an overview of the Irumide belt, based on previously published and new geological, geochronological and geochemical data, and attempts to place this tectonic unit in a regional context.

2. Tectonostratigraphy and geochronology

2.1. General location of units

Fig. 2 presents a simplified geological map of the foreland to the Irumide belt in northern Zambia. Figs. 3 and 4 are simplified maps of the southwestern and northeastern Irumide belt respectively, indicating the location of geological maps published by the Geological Survey Department of Zambia and used in this review. Fig. 5 is a location map of the main geochronological data reported in the paper, and the approximate position of Figs. 2–4 and 6–10. Fig. 5 also shows the location of what in this paper is termed the Bangweulu block, Irumide belt s.s. and southeastern Irumide belt. The large number of new U–Pb SHRIMP data acquired in the Irumide belt s.s. are displayed in Figs. 6–10, together with a few previous whole-rock Rb–Sr isochron dates used in the text. All ages reported in the text and shown on the figures are summarised in Table 1 where the sources of the geochronological data are listed. All these data were calculated (or recalculated where necessary) using decay constants of Steiger and Jäger (1977).

2.2. Basement

Earlier workers have indicated that the Irumide belt overlies an Archaean/Palaeoproterozoic basement (e.g.

Table 1
Geochronological data on rocks of the Irumide belt and associated basement

No.	ID	Rock type	Age ± error (Ma)	Method	Source
1		Volcanics	596 ± 10	WR Rb–Sr isochron	Haslam et al. (1986)
2	LW2	Luswa Syenite	943 ± 5	U-Pb SHRIMP zircon	De Waele et al. (2003c)
3		Lufila Granite	947 ± 89	WR Rb–Sr isochron	Daly (1986)
4		Kaunga Granite	970 ± 5	TIMS bulk zircon	Daly (1986)
5		Aplite in Luromo Granite	977 ± 1	Pb evaporation	Ring et al. (1999)
6		Aplite in Wililo Granite	983 ± 1	Pb evaporation	Ring et al. (1999)
7	SH8	Lufila Granite	1001 ± 44	U-Pb SHRIMP zircon	De Waele (2005)
8		Luangwa Gneiss	~2033	LA-ICP-MS	Cox et al. (2002)
9	LW1	Chilubanama Granite	1005 ± 21	U-Pb SHRIMP zircon	De Waele (2005)
10	KK1	Porphyritic granite	1003 ± 31	U-Pb SHRIMP zircon	De Waele (2005)
11	CHT6	Biotite granite gneiss	1005 ± 7	U-Pb SHRIMP zircon	De Waele (2005)
12	MTG4	Chilubanama Granite	1010 ± 11	U-Pb SHRIMP zircon	De Waele et al. (2003c)
	MTG4[a]	Chilubanama Granite	*1004 ± 16*	U-Pb SHRIMP zircon	De Waele et al. (2003c)
13	SER6-5	Lukusahi migmatite	*1018 ± 5*	U-Pb SHRIMP zircon	De Waele et al. (2003c)
14	SASA2	Sasa Granite	1016 ± 14	U-Pb SHRIMP zircon	De Waele et al. (2003c)
15	CHL5	Granite gneiss	1016 ± 17	U-Pb SHRIMP zircon	De Waele (2005)
16	SER6-7[b]	Fukwe Migmatite	*1021 ± 16*	U-Pb SHRIMP zircon	De Waele et al. (2003c)
	SER6-7[b]	Fukwe Migmatite	*554* ± 20	U-Pb SHRIMP zircon	De Waele (2005)
17	KN8	Biotite granite gneiss	1022 ± 16	U-Pb SHRIMP zircon	De Waele (2005)
18	ND1	Porphyritic granite	1023 ± 7	U-Pb SHRIMP zircon	De Waele (2005)
19	ZM36	Mununga Quarry Granite	1025 ± 10	U-Pb SHRIMP zircon	De Waele et al. (2003c)
20	MTGG1	Mutangoshi Gneissic Granite	1027 ± 13	U-Pb SHRIMP zircon	De Waele et al. (2003c)
21	ND5	Syeno-granite	1028 ± 7	U-Pb SHRIMP zircon	De Waele (2005)
22	MH9C	Porphyritic granite	1029 ± 14	U-Pb SHRIMP zircon	De Waele (2005)
23	KN2A	Porphyritic granite	1031 ± 14	U-Pb SHRIMP zircon	De Waele (2005)
24	MH4	Porphyritic granite	1017 ± 19	U-Pb SHRIMP zircon	De Waele (2005)
25	SQG	Serenje Quarry Granite	1024 ± 9	U-Pb SHRIMP zircon	De Waele et al. (2003c)
26	SER5-3	Porphyritic granite	1034 ± 5	U-Pb SHRIMP zircon	De Waele et al. (2003c)
27	CC8	Porphyritic granite	1035 ± 12	U-Pb SHRIMP zircon	De Waele (2005)
28	SER6-4	Porphyritic granite	1036 ± 13	U-Pb SHRIMP zircon	De Waele et al. (2003c)
29	ND4	Granodiorite	1035 ± 19	U-Pb SHRIMP zircon	De Waele (2005)
30	CC5	Porphyritic granite	1038 ± 17	U-Pb SHRIMP zircon	De Waele (2005)
31	FW1	Porphyritic granite	1038 ± 58	U-Pb SHRIMP zircon	De Waele (2005)
32	ZAM5	Chipata Granite	1041 ± 9	U-Pb SHRIMP zircon	De Waele (2005)
33		Luangwa gneiss	*1043 ± 19*	LA-ICP-MS	Cox et al. (2002)
34		Chipata granulite	*1046* ± 3	TIMS single monazite	Schenk and Appel (2001)
35	ZAM1	Chipata granulite	*1047 ± 20*	U-Pb SHRIMP zircon	De Waele (2005)
36	KN7	Porphyritic granite	1048 ± 10	U-Pb SHRIMP zircon	De Waele (2005)
37	ZAM4	Chipata Granite	1050 ± 10	U-Pb SHRIMP zircon	De Waele (2005)
38	KN3	Biotite granite gneiss	1053 ± 14	U-Pb SHRIMP zircon	De Waele (2005)
39	MTGG2	Mutangoshi Gneissic Granite	1055 ± 13	U-Pb SHRIMP zircon	De Waele et al. (2003c)
40	ZAM3	Chipata Granite	1076 ± 3	U-Pb SHRIMP zircon	De Waele (2005)
41		Lwakwa granite	1087 ± 11	TIMS single zircon	Ring et al. (1999)
42		Mkushi gneiss	1088 ± 159	U-Pb SHRIMP zircon	Rainaud et al. (2002)
43		Luromo granite	1108 ± 1	Pb evaporation	Ring et al. (1999)
44		Wililo granite	1115 ± 1	Pb evaporation	Ring et al. (1999)
45		Wililo granite	1116 ± 1	Pb evaporation	Ring et al. (1999)
46		Wililo granite	1118 ± 1	Pb evaporation	Ring et al. (1999)
47		Mwenga granite	1119 ± 20	TIMS single zircon	Ring et al. (1999)
48		Lusenga syenite	1145 ± 20	WR Rb–Sr isochron	Brewer et al. (1979)
49		Semahwa gneiss	1198 ± 6	TIMS bulk zircon	Hanson et al. (1988)
50		Chilala gneiss	1285 ± 64	TIMS bulk zircon	Hanson et al. (1988)
51		Ntendele metatonalite	1329 ± 1	Pb evaporation	Vrána et al. (2004)
52		Mivula syenite	1341 ± 16	WR Rb–Sr isochron	Tembo (1986)
53		Zongwe gneiss	1343 ± 6	TIMS bulk zircon	Hanson et al. (1988)
54		Siasikabole granite	1352 ± 14	TIMS bulk zircon	Hanson et al. (1988)
55		Mivula syenite	1360 ± 1	Pb evaporation	Vrána et al. (2004)
56		Mutangoshi gneiss	1407 ± 33	WR Rb–Sr isochron	Daly (1986)
57	ML2	Lubu Granite Gneiss	1551 ± 33	U-Pb SHRIMP zircon	De Waele et al. (2003c)
58	LW10	Musalango Gneiss	1610 ± 26	U-Pb SHRIMP zircon	De Waele et al. (2003c)
59	ND2	Granite gneiss	1627 ± 12	U-Pb SHRIMP zircon	De Waele (2005)
60	SR12	Lukamfwa Hill Granite Gneiss	1639 ± 14	U-Pb SHRIMP zircon	De Waele et al. (2003c)
61	SER6-3	Lukamfwa Hill Granite Gneiss	1652 ± 6	U-Pb SHRIMP zircon	De Waele et al. (2003c)
62	SER6-2	Lukamfwa Hill Granite Gneiss	1664 ± 4	U-Pb SHRIMP zircon	De Waele et al. (2003c)

(continued on next page)

Table 1 (*continued*)

No.	ID	Rock type	Age ± error (Ma)	Method	Source
63		Luchewe granite	1780 ± 250	WR Rb-Sr isochron	Schandelmeier (1980)
64		Mansa volcanic	1815 ± 29	WR Rb-Sr isochron	Brewer et al. (1979)
65		Kate granite	1830 ± 85	WR Rb-Sr isochron	Schandelmeier (1980)
66		Mansa granite	1852 ± 52	WR Rb-Sr isochron	Brewer et al. (1979)
67	IS20	Kachinga Tuff	1856 ± 4	U–Pb SHRIMP zircon	De Waele (2005)
68	MA1	Mansa Granite	1860 ± 13	U–Pb SHRIMP zircon	De Waele (2005)
69	MA5	Mansa Volcanic	1862 ± 19	U–Pb SHRIMP zircon	De Waele (2005)
70	MA2	Mansa granite	1862 ± 8	U–Pb SHRIMP zircon	De Waele (2005)
71	MA9	Musonda Falls Granite	1866 ± 9	U–Pb SHRIMP zircon	De Waele (2005)
72	MA3	Mansa Volcanic	1868 ± 7	U–Pb SHRIMP zircon	De Waele (2005)
73	KB5	Katibunga Basalt	1871 ± 24	U–Pb SHRIMP zircon	De Waele (2005)
74		Kinsenda Lufubu schist	1873 ± 8	U–Pb SHRIMP zircon	Rainaud et al. (2002)
75		Solwezi granite	1874 ± 9	TIMS single zircon	John (2001)
76		Mambwe gneiss	1877 ± 55	WR Rb-Sr isochron	Schandelmeier (1980)
77	ZM31	Luswa River Tuff	1879 ± 13	U–Pb SHRIMP zircon	De Waele (2005)
78		Kinsenda granite (Luina dome)	1882 ± 20	TIMS single zircon	Ngoyi et al. (1991)
79		Kabompo granite	1884 ± 10	TIMS single zircon	John (2001)
80	ISK2	Luwalizi Granite Gneiss	1927 ± 10	U–Pb SHRIMP zircon	De Waele (2005)
81		Nyika granite	1932 ± 9	TIMS bulk zircon	Dodson et al. (1975)
82	ISK1	Luwalizi Granite Gneiss	1942 ± 6	U–Pb SHRIMP zircon	De Waele (2005)
83	CC10	Porphyritic granite gneiss	1953 ± 6	U–Pb SHRIMP zircon	De Waele (2005)
84		Biotite metatonalite	1961 ± 1	Pb evaporation	Vrána et al. (2004)
85		Samba porphyry	1964 ± 12	U–Pb SHRIMP zircon	Rainaud et al. (2002)
86		Lufubu schist	1970 ± 10	U–Pb SHRIMP zircon	Rainaud et al. (2002)
87		Nyika granite	1969 ± 1	Pb evaporation	Ring et al. (1997)
88	ZAM2	Lutembwe River Granulite	1974 ± 18	U–Pb SHRIMP zircon	De Waele (2005)
89		Mulungushi gneiss	1976 ± 5	U–Pb SHRIMP zircon	Rainaud et al. (2002)
90		Chambishi granite	1980 ± 7	U–Pb SHRIMP zircon	Rainaud et al. (2002)
91		Chambishi granite	1983 ± 5	U–Pb SHRIMP zircon	Rainaud et al. (2002)
92		Rufiphi granite	1988 ± 1	Pb evaporation	Ring et al. (1997)
93		Mufulira granite	1991 ± 3	U–Pb SHRIMP zircon	Rainaud et al. (2002)
94		Chelinda granite	1995 ± 1	Pb evaporation	Ring et al. (1997)
95		Lurumo granite	2002 ± 1	Pb evaporation	Ring et al. (1997)
96		Luangwa granite	~2033	LA-ICP-MS	Cox et al. (2002)
97	MK3	Mkushi Gneiss	2042 ± 10	U–Pb SHRIMP zircon	De Waele (2005)
98	MK5	Mkushi Gneiss	2029 ± 7	U–Pb SHRIMP zircon	De Waele (2005)
	MK5	Mkushi Gneiss	2050 ± 9	U–Pb SHRIMP zircon	
99	KN1	Mkushi Gneiss	2036 ± 6	U–Pb SHRIMP zircon	De Waele (2005)
100		Rufiphi granite	2048 ± 1	Pb evaporation	Ring et al. (1997)
101		Mkushi gneiss	2049 ± 9	U–Pb SHRIMP zircon	Rainaud et al. (2002)
102		Mwinilunga granite	2058 ± 7	U–Pb SHRIMP zircon	Key et al. (2001)
103		Lurumo granite	2093 ± 1	Pb evaporation	Ring et al. (1997)
104		Lurumo granite	2224 ± 1	Pb evaporation	Ring et al. (1997)
105		Mwinilunga granite	2538 ± 10	U–Pb SHRIMP zircon	Key et al. (2001)
106		Mwinilunga granite	2543 ± 5	U–Pb SHRIMP zircon	Key et al. (2001)
107		Mwinilunga granite	2561 ± 10	U–Pb SHRIMP zircon	Key et al. (2001)
108		Luangwa gneiss	2608 ± 14	LA-ICP-MS	Cox et al. (2002)
109	KMP1	Kapiri Mposhi Granite	2726 ± 36	U–Pb SHRIMP zircon	De Waele (2005)
110		Chembeweu Quartzite	Detrital	U–Pb SHRIMP zircon	De Waele (2005)
111		Mufulira quartzite	Detrital	U–Pb SHRIMP zircon	Rainaud et al. (2002)
112		Kasama quartzite	Detrital	U–Pb SHRIMP zircon	De Waele (2005)
113		Mansa quartzite	Detrital	U–Pb SHRIMP zircon	De Waele (2005)

Ages interpreted to date peak metamorphism are in italics.
No. refers to numbers mentioned in the text, ID refers to sample names of own samples.

Drysdall et al., 1972; Daly, 1986). An extensive set of new sensitive high-mass resolution ion microprobe (SHRIMP) U–Pb zircon geochronological data (Table 1) is used in this paper to constrain the age of crustal rocks affected by the Irumide contractional deformation and those exposed in the Irumide foreland. The main basement lithologies exposed in and adjacent to the Irumide belt are described below according to geographic location, from the northeast (the Bangweulu block and related basement lithologies in the Irumide belt, Fig. 2) to the centre (basement lithologies in the Irumide belt s.s., Figs. 3, 4, 6–10), southwest (Domes of the Copperbelt area, Fig. 5) and southeast (Lutembwe Granulite near Chipata and the Nyika Granite (NG), Fig. 5) near the Malawi border. This section includes data

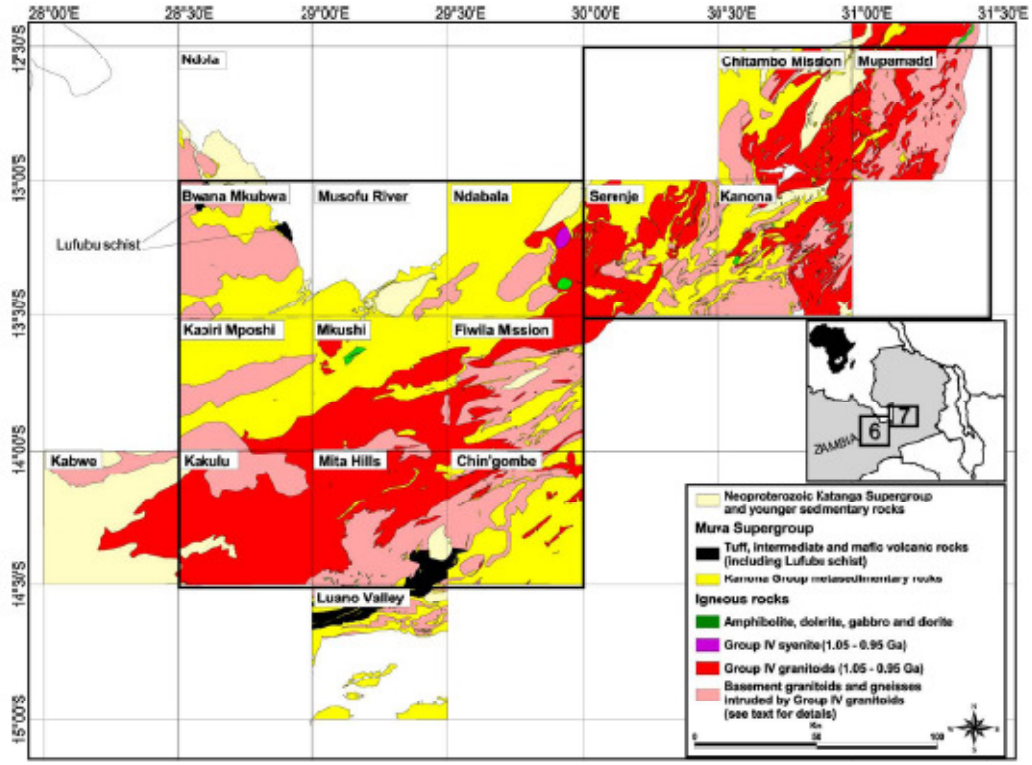

Fig. 3. Overview map of the southwestern Irumide belt, showing simplified geology and the location of mapped quarter-degree sheets. The simplified geology is adapted from the 1:1,000,000 geological map of Zambia (Thieme and Johnson, 1981).

related to correlative basement units within the Irumide belt and Copperbelt (outside the Irumide belt s.s.) that have a major bearing on proving that basement lithologies underlie large portions of the Irumide belt.

2.2.1. Bangweulu block

The Bangweulu block comprises three distinct lithotectonic units (Fig. 2): (1) a series of northwest-trending high-grade metapelites exposed in northeast Zambia and within the Palaeoproterozoic Ubendian belt; (b) a series of east–west-trending schist belts on the Bangweulu block known as the Mulungwizi Gneisses (Namateba, 1994; Van Tuijl and Verhoog, 1995; Verhoog and Van Tuijl, 1995a,b,c); (c) an extensive suite of plutono-volcanics overlain by the supracrustal Mporokoso Group metasedimentary sequence (Andersen and Unrug, 1984; Andrews-Speed, 1989).

The main lithology of the Mulungwizi Gneiss consists of migmatitic biotite gneiss, with minor biotite-epidote and muscovite gneiss, associated with mica-schist, amphibolite and quartzite. The main fabric of the Mulungwizi Gneiss strikes east–southeast with steep dips to both the north–northeast and south–southwest. The Mulungwizi Gneiss is reported to pass eastwards into Palaeoproterozoic gneiss of the Ubendian belt with no obvious break; they are therefore inferred to be correlatives (Namateba, 1994; Van Tuijl and Verhoog, 1995; Verhoog and Van Tuijl, 1995a,b,c). Pelitic schist belts exposed farther west in the Bangweulu block display a similar east–southeast-fabric to the Mulungwizi Gneiss, from which they are separated by relatively undeformed granitoids of the Bangweulu block, one of which yielded a Rb–Sr date of 1877 ± 55 Ma (Schandelmeier, 1981, see Fig. 5 and Table 1, no. 76). The schist belts are interpreted as vestiges of the Palaeoproterozoic Ubendian belt in the Bangweulu block (Namateba, 1994; Van Tuijl and Verhoog, 1995; Verhoog and Van Tuijl, 1995a,b,c).

In the northwestern part of the Bangweulu block, the contact between plutono-volcanic rocks and the Mporokoso Group supracrustal metasedimentary sequence is a high-strain zone, locally known as the Luongo Shear Zone (Fig. 2). The Bangweulu block high-K calc-alkaline felsic igneous rocks represent a continental arc related to the

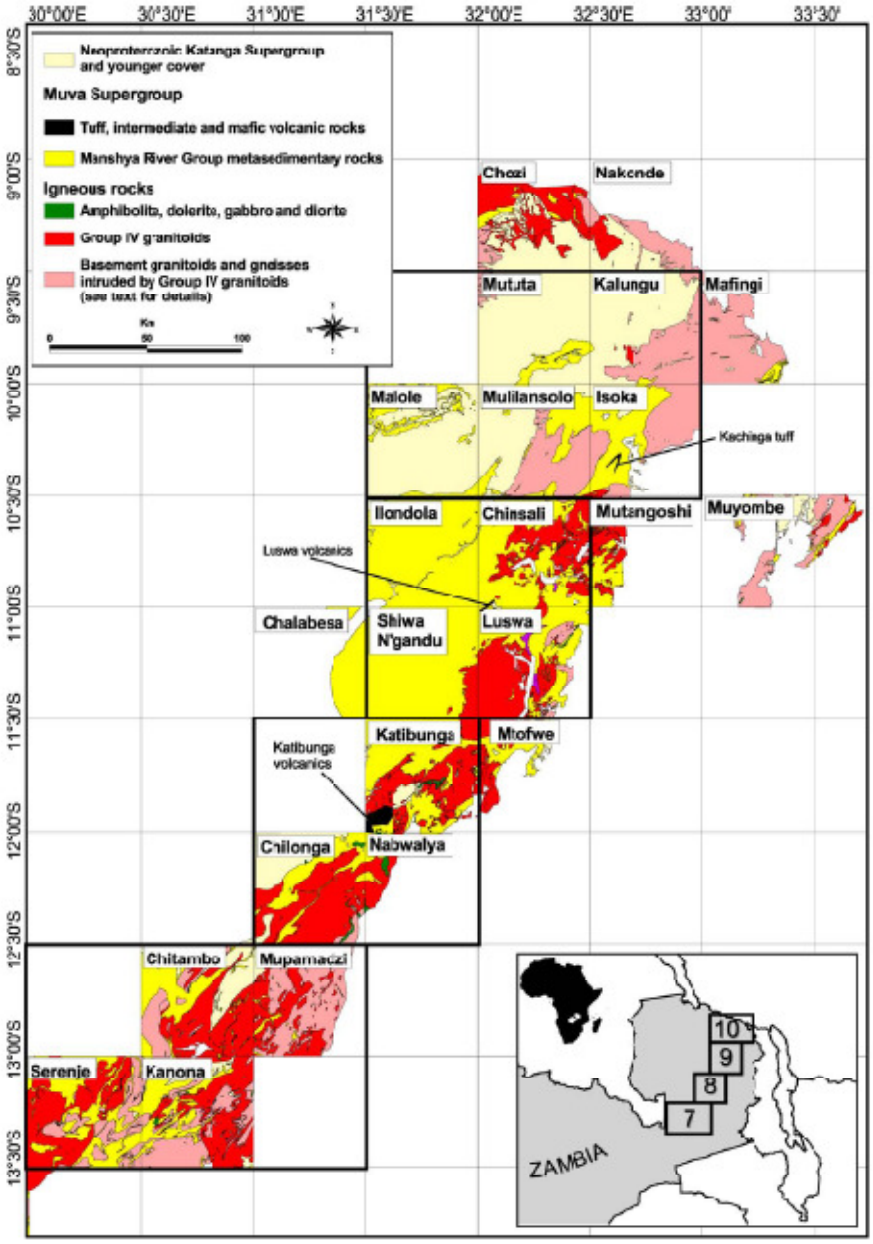

Fig. 4. Overview map of the northeastern Irumide belt, showing simplified geology and the location of mapped quarter-degree sheets. The simplified geology is adapted from the 1:1,000,000 geological map of Zambia (Thieme and Johnson, 1981).

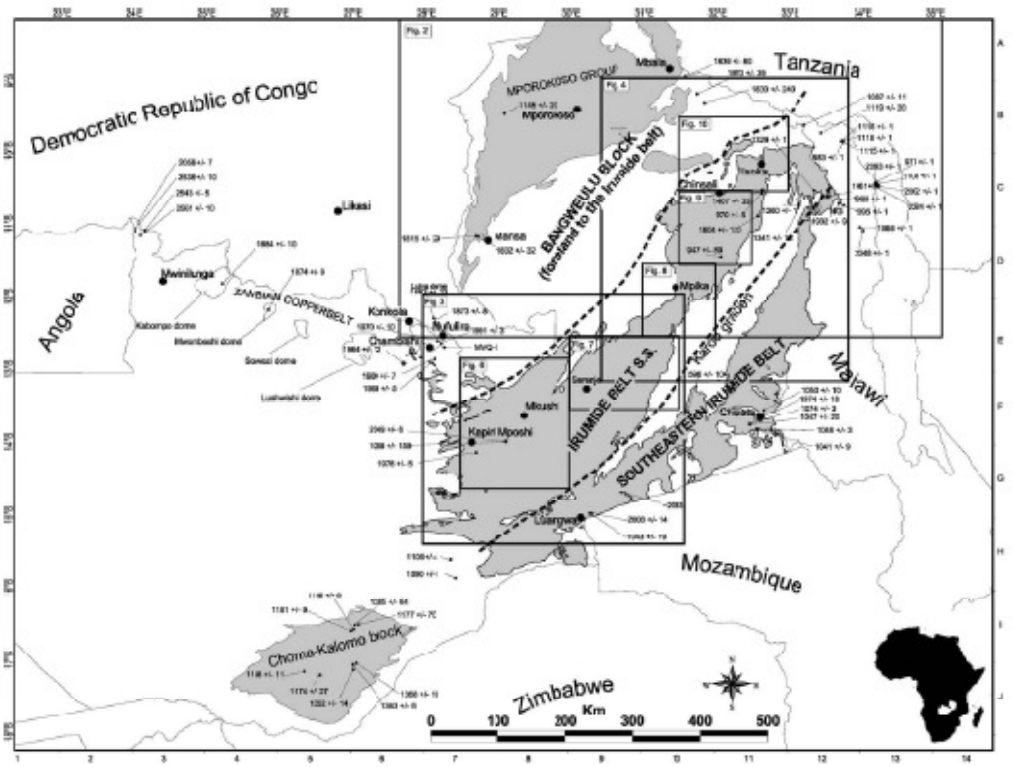

Fig. 5. Overview of previously published Proterozoic age data for Zambia (refer to Table 1 for sources of data). The locations of Figs. 2–4 and 6–10 are indicated.

Ubendian belt (Brewer et al., 1979; Andersen and Unrug, 1984; Kabengele et al., 1991). Rb–Sr whole-rock dates on granitoids and rhyolites suggest the emplacement of the suite between 1.88 and 1.82 Ga (Brewer et al., 1979; Schandelmeier, 1981, 1983, Fig. 5, Table 1, nos. 63–66 and 76). SHRIMP U–Pb zircon dating of Bangweulu block igneous rocks exposed near Mansa (Fig. 2) yielded dates of 1890 ± 13, 1862 ± 8 and 1866 ± 9 Ma for granitoids and 1858 ± 7 and 1862 ± 19 Ma for rhyolites (De Waele et al., 2003b, 2005; De Waele and Fitzsimons, submitted for publication, Table 1, nos. 68–72). These dates supersede previous estimates on the emplacement of these granites and associated volcanic rocks (Brewer et al., 1979).

Two granites exposed within the northeastern part of the Irumide belt (the Luwalizi Granite near Isoka, Fig. 4) yielded SHRIMP U–Pb zircon dates of 1942 ± 6 and 1927 ± 10 Ma (De Waele et al., 2003b; De Waele and Fitzsimons, submitted for publication, Fig. 10, Table 1, nos. 80 and 82) and form part of a Palaeoproterozoic basement to the Irumide belt. The Luwalizi granites are mildly deformed biotite granites, and are structurally overlain by the Manshya River Group metasedimentary succession of the northeastern Irumide belt.

2.2.2. Mkushi Gneiss Complex

The Mkushi Gneiss Complex comprises banded biotite gneisses, augen gneisses and porphyritic granite gneisses, collectively known as the Mkushi Gneiss, underlying the southwestern Irumide belt (Stillman, 1965, Figs. 6 and 7). The Mkushi Gneiss yielded a SHRIMP U–Pb zircon igneous crystallisation age of 2049 ± 6 Ma on a sample from the Munshiwemba Quarry south of Mkush (Rainaud et al., 2002, 2003, Fig. 6, Table 1, no. 101). At Munshiwemba Quarry, the Mkushi Gneiss is a highly sheared biotite-rich, coarse porphyritic and medium-grained granite, which yielded SHRIMP U–Pb zircon dates of 2042 ± 10 and 2029 ± 7 Ma (De Waele et al., 2003a,b, Fig. 6, Table 1, nos. 97 and 98). It is cut by aplite veins containing inherited zircons with cores yielding the same date as the Mkushi Gneiss, and magmatic overgrowths yielding a low-precision date of 1088 ± 159 Ma (Rainaud et al., 2002, 2003, 2005, Fig. 6, Table 1, no. 42). Farther to the

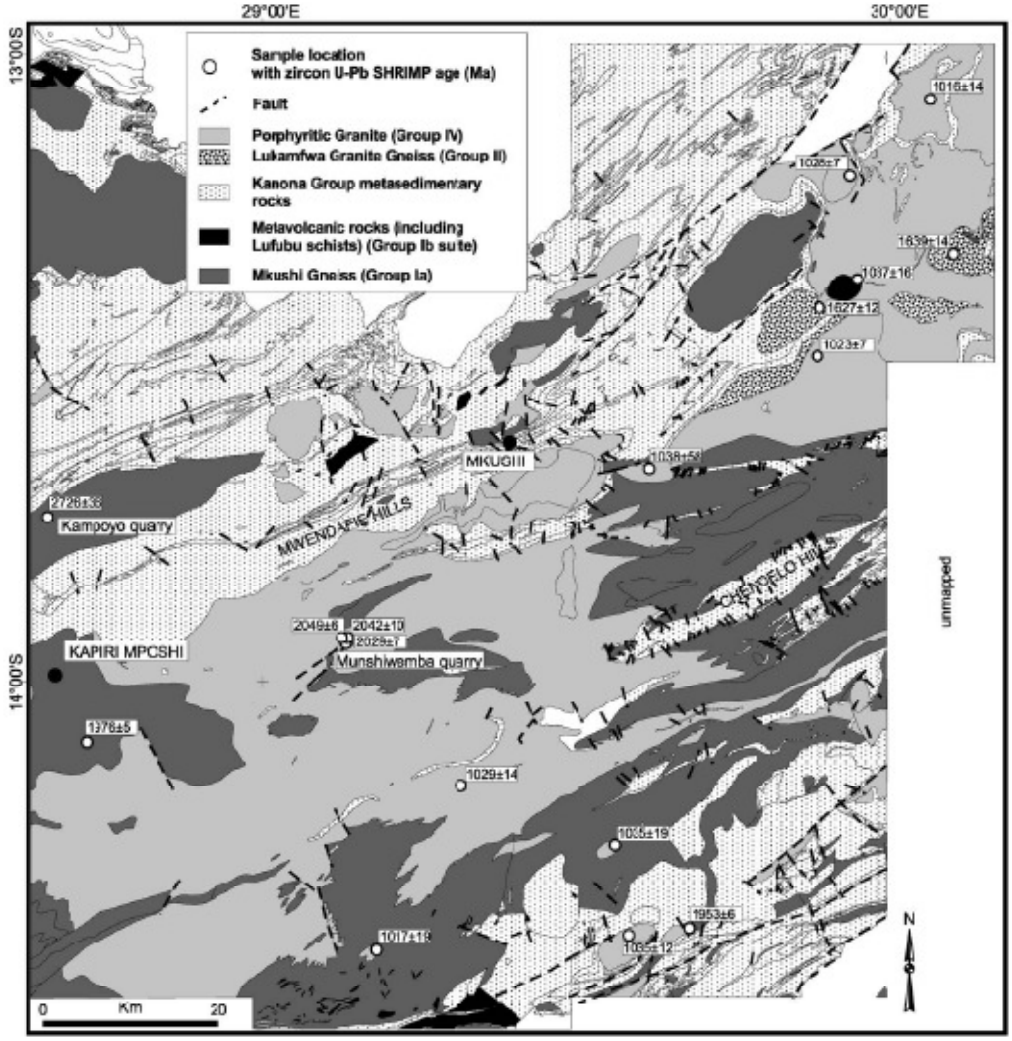

Fig. 6. Simplified geological map of the area around Mkushi, based on published 1:100,000 scale geological maps; includes Kapiri Mposhi, Kabulu (Mulungushi), Mita Hills, Mkushi, Musofu River, Fiwila and Ndabala map sheets and parts of Serenje, Chin'gombe, Luano and Bwana Mkubwa map sheets (Stillman, 1965; Smith, 1966; Moore, 1967; Cvetcovic, 1973; Kerr, 1975; Smith and Kerr, 1975; Reichwalder and Brandon, 1992; Mapani and Moore, 1995; Carruthers, 2000; Chisela, 2000).

southwest, a megacrystic granite yielded a SHRIMP U–Pb zircon igneous crystallisation age of 1976 ± 5 Ma (Rainaud et al., 2002, Fig. 6, Table 1, no. 89). To the northeast, a biotite granite gneiss in the Kanona area yielded a SHRIMP U–Pb zircon igneous crystallisation age of 2036 ± 6 Ma (Fig. 7, Table 1, no. 99), while to the southeast of the Munshiwemba Quarry, a porphyritic biotite granite gneiss from Chin'gombe Mission was emplaced at 1953 ± 6 Ma (De Waele et al., 2003a,b, Fig. 6, Table 1, no. 83). The data in Table 1 confirm the presence of a Palaeoproterozoic (2.05–1.95 Ga) basement throughout the southwestern Irumide belt, which is collectively ascribed to the Mkushi Gneiss Complex. Granitoids intruding the Mkushi Gneiss Complex and previously mapped as part of this complex (Smith, 1966; Cvetcovic, 1973; Page, 1973; Kerr, 1975; Smith and Kerr, 1975) yielded SHRIMP U–Pb zircon

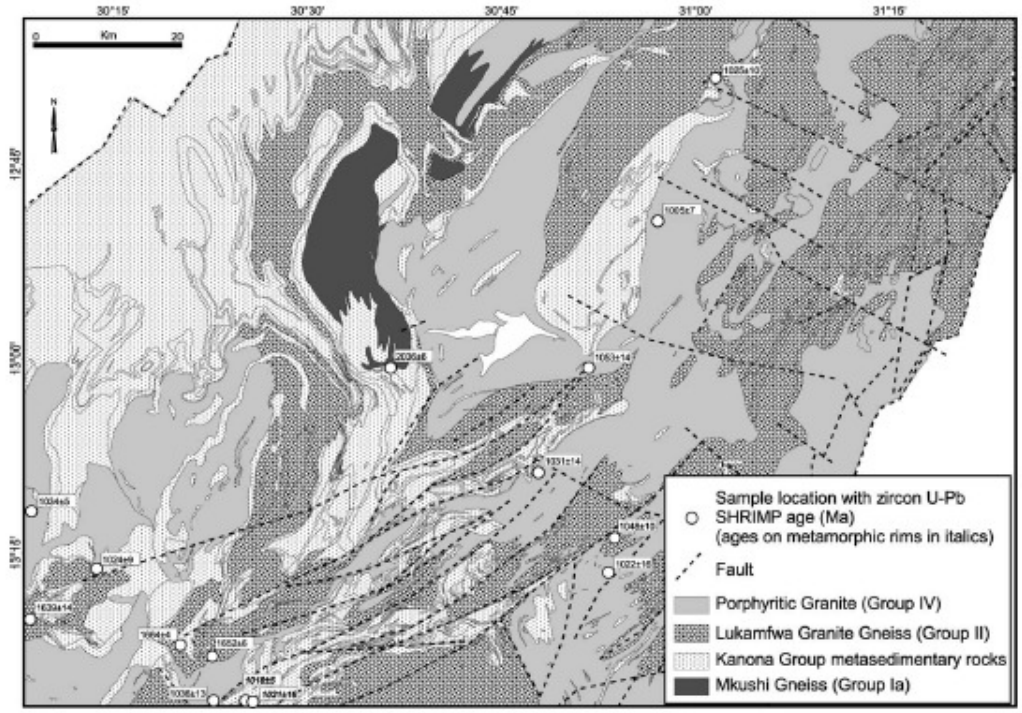

Fig. 7. Simplified geological map of the region around Kanona, adapted from published 1:100,000 scale geological maps; includes Kasanka (mapped from satellite imagery), Serenje, Kanona, Chitambo, and Mupamadzi sheets (Cordiner, 1977; Mapani and Moore, 1995; Van de Velde and De Waele, 1997; Cordiner, 2000).

igneous crystallisation ages of ca. 1.65 and 1.05–1.02 Ga (De Waele et al., 2003c).

2.2.3. Copperbelt domes

In the Copperbelt, basement "Domes" (Fig. 5) contain migmatites, gneisses and deformed granites exposed in the Lushwishi, Konkola, Luina, Solwezi, Mwombeshi and Kabompo Domes in Zambia and southern Katanga (Democratic Republic of Congo, hereafter DRC). The Luina Dome granites yielded a thermal ionisation mass spectrometry (TIMS) U–Pb zircon date of 1882 ± 20 Ma (Ngoyi et al., 1991, Fig. 5, Table 1, no. 78). John (2001) reported TIMS U–Pb zircon dates of 1874 ± 9 Ma for a granite of the Solwezi Dome and 1884 ± 10 Ma for a granite of the Kabompo Dome (Fig. 5, Table 1, nos. 75 and 79). Rainaud et al. (2002) reported SHRIMP U–Pb zircon emplacement ages of 1991 ± 3 Ma for the Mufulira Granite, 1983 ± 5 and 1980 ± 7 Ma for the granite underlying the Chambishi basin in the Copperbelt (Fig. 5, Table 1, nos. 90, 91 and 93). Two samples of the Lufubu metavolcanic schist, one from DRC and one from Zambia, yielded SHRIMP U–Pb igneous crystallisation ages of 1873 ± 8 and 1970 ± 10 Ma respectively (Rainaud et al., 2002, Fig. 5, Table 1, nos. 74 and 86 respectively). Key et al. (2001) reported SHRIMP U–Pb zircon emplacement ages of 2543 ± 5, 2561 ± 10, 2538 ± 10 and 2058 ± 7 Ma for pre-Neoproterozoic basement granitoids bounding the Zambian Copperbelt to the northwest (Fig. 5, Table 1, nos. 105–107 and 102). These late Archaean granitoids were interpreted to form part of the Congo craton in northwest Zambia (Key et al., 2001). Apart from the Neoarchaean lithologies in the far western portion, the Copperbelt area appears to be underlain by a Palaeoproterozoic basement with igneous crystallisation ages between 2.06 and 1.87 Ga.

2.2.4. Chipata area and eastern extension of the Irumide belt

Pre-Irumide rocks exposed within the southeastern Irumide belt include a granodioritic gneiss from the Luangwa area recording a laser ablation-inductively coupled plasma–mass spectrometry (LA–ICP–MS) U–Pb zircon date of 2608 ± 14 Ma (Cox et al., 2002, Fig. 5, Table 1, no. 108). A foliated granite gneiss from the same area

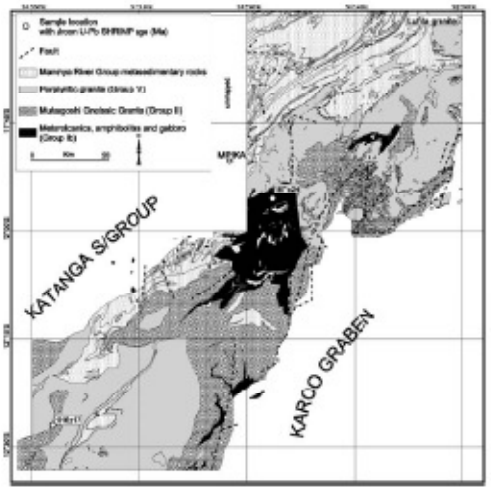

Fig. 8. Simplified geological map of the region around Mpika, adapted from published 1:100,000 scale geological maps; includes Chilonga Mission and Kanitunga Mission areas and parts of Mtotwe and Mupamadzi River areas (Cordiner, 1977; Mosley, 1979; Mosley and Marten, 1979; Van ce Velde and De Waele, 1997).

yielded a LA–ICP–MS zircon U–Pb date of ~2033 Ma (Cox et al., 2002, Fig. 5, Table 1, no. 96). The Lutembwe River granulite in the Chipata area (eastern Zambia) yielded a SHRIMP U–Pb protolith age of 1974 ± 18 Ma (De Waele, 2005, Fig. 5, Table 1, no. 88). This age supersedes a Rb–Sr whole rock-biotite date of 2117 ± 15 Ma previously reported by Liyungu and Vinyu (1996), and a low-precision Rb–Sr whole-rock date of 2290 ± 240 Ma ($(^{87}Sr/^{86}Sr)_i = 0.7145 \pm 0.0091$) reported by Haslam et al. (1986). The Nyika granite (Malawi) yielded a bulk U–Pb zircon date of 1932 ± 9 Ma (recalculated from Dodson et al., 1975, Fig. 5, Table 1, no. 81). Ring et al. (1997) reported a $^{207}Pb/^{206}Pb$ zircon evaporation date of 1969 ± 1 Ma for a granite exposed to the north of the Nyika pluton, providing a more reliable estimate for the emplacement age of the suite (Fig. 5, Table 1, no. 87). Ring et al. further reported a number of $^{207}Pb/^{206}Pb$ zircon evaporation dates between 2093 and 1988 Ma in northern Malawi, and interpreted a $^{207}Pb/^{206}Pb$ zircon date of 2002 ± 1 Ma on metamorphic zircon to constrain peak Ubendian metamorphism (Ring et al., 1997, Fig. 5, Table 1, nos 92, 94, 95, 100, 103 and 104). A biotite metatonalite intruding the granulites of the Muyombe area in northeast Zambia yielded a $^{207}Pb/^{206}Pb$ zircon evaporation date of 1961 ± 1 Ma (Vrána et al., 2004, Fig 5, Table 1, no. 84).

2.2.5. Summary on the basement

Basement is exposed north and northwest of the Irumide belt and comprises of Palaeoproterozoic plutono-volcanic rocks and gneisses emplaced between 2.05 and 1.85 Ga. This basement is part of the Bangweulu block.

To the west, the Copperbelt Domes include variably deformed granitoids and (meta)volcanic units also emplaced between ca. 2.06–1.87 Ga taken to represent the westward continuation of the Palaeoproterozoic Bangweulu block within the Neoproterozoic Lufilian belt.

To the south and southeast, pre-Irumide lithologies comprise a Neoarchaean unit with igneous crystallisation age of ca. 2.61 Ga, and various gneisses with protolith igneous crystallisation ages between 2.03 and 1.97 Ga. However, at present it is unclear whether these lithologies represent the southerly extension of the Bangweulu block in the Irumide belt or whether they represent distinct crustal blocks accreted to the southern margin of the Bangweulu block during the Irumide orogeny.

2.3. Muva supergroup

2.3.1. Introduction

The Muva of Ackermann (1950, 1960) and Ackermann and Forster (1960), which included only the sedimentary units identified in the Irumide belt s.s., has been redefined to include the post-2000 Ma sedimentary cover of the Bangweulu block (Daly and Unrug, 1982). To the north of the Karoo-age Luangwa graben (Karoo graben in Fig. 5), three different supracrustal sedimentary successions form the Muva Supergroup (Fig. 11), and include the Mporokoso Group of northern Zambia, the Kasama Formation of the Kasama area, and the Manshya River and Mitoba River Groups of the Irumide belt (Daly and Unrug, 1982). The Manshya River Group is a lateral correlative of the Kanona Group in the southwestern Irumide belt (De Waele and Mapani, 2002), which comprises the previously defined Irumi, Musofu and Kalonga Formations of Sullivan (1965). Direct member-to-member correlation of the Manshya River Group with the Mafing Group of Fitches (1968, 1971) to the northeast is not possible, but is inferred from broad lithological and structural similarities. South of the Luangwa graben (Karoo graben in Fig 5) an extensive ridge-forming quartzite-metapelite succession and a thick carbonate sequence are ascribed to the Muvuye, Sinda and Sasare Groups (Phillips, 1960, 1964, 1965; Barr and Drysdall, 1972; Agar and Ray, 1983). Although no direct correlation can be supported, this sedimentary package was regarded as a deep marine distal facies of the Manshya River Group (Daly and Unrug, 1982; Daly, 1986). The different lithostratigraphic units are described below from north to south, while simplified stratigraphic columns are shown in Fig. 12.

2.3.2. Mporokoso Group

The Mporokoso Group was extensively described by Andrews-Speed and Unrug (1982), Daly and Unrug (1982), Andersen and Unrug (1984), Unrug (1984) and Andrews-Speed (1986, 1989), and comprises a mildly

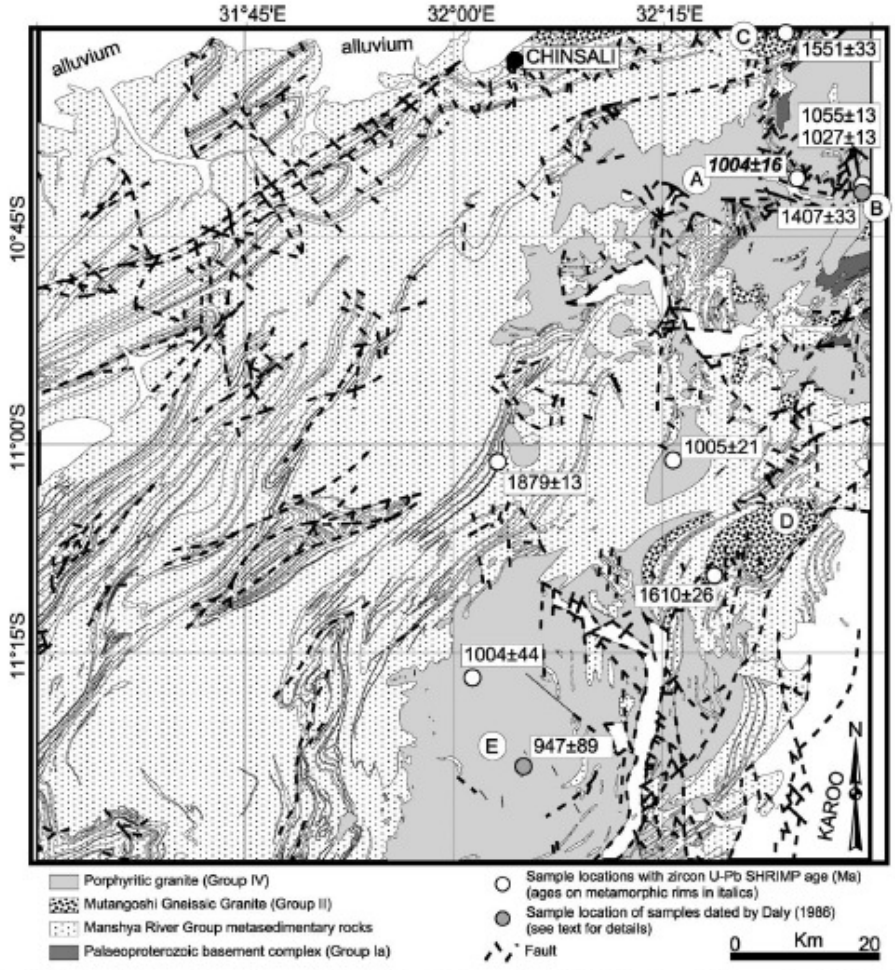

Fig. 9. Simplified geological map of the region around Chinsali, adapted from published 1:100,000 scale geological maps; includes Shiwa N'gandu, Ilondola Mission, Luswa River and Chinsali map sheets (Daly, 1994a; Sykes, 1995; Ayres, 1974; Lucacik, 1998). A = Chilubanama Granite; B = Mutangoshi Gneissic Granite; C = Lubu Granite Gneiss; D = Musalango Gneiss; E = Lufila Granite (Bemba Batholith).

deformed and low-grade 5000-m-thick sedimentary package subdivided into four formations (Fig. 12). The oldest, the Mbala Formation, contains volcanic rocks but consists mainly of conglomerate/diamictite, feldspathic sandstone, orthoquartzite, purple pelite and silicified tuff. The thickness of the sequence increases from 250 m in the south near Mansa to 2700 m in the north near Mbala. The Mbala Formation is overlain by up to 600 m of shales and tuffs of the Nsama Formation, which is locally absent in the south. The Kabweluma Formation consists of a ~1500-m-thick sequence of fluviatile quartzites and minor mudstones. The uppermost Chibote Formation comprises of ~100 m of mudstones. Andersen and Unrug (1984) pointed out that palaeocurrent directions indicate a sediment source to the south (present coordinates).

2.3.3. Kasama Formation

The Kasama Formation occurs only in a small basin in the eastern part of the Bangweulu block (Fig. 2). At its type locality east of Kasama (Unrug, 1982), the sequence consists mainly of mature quartzites, with subordinate mudstones. The mature character of the Kasama quartzites

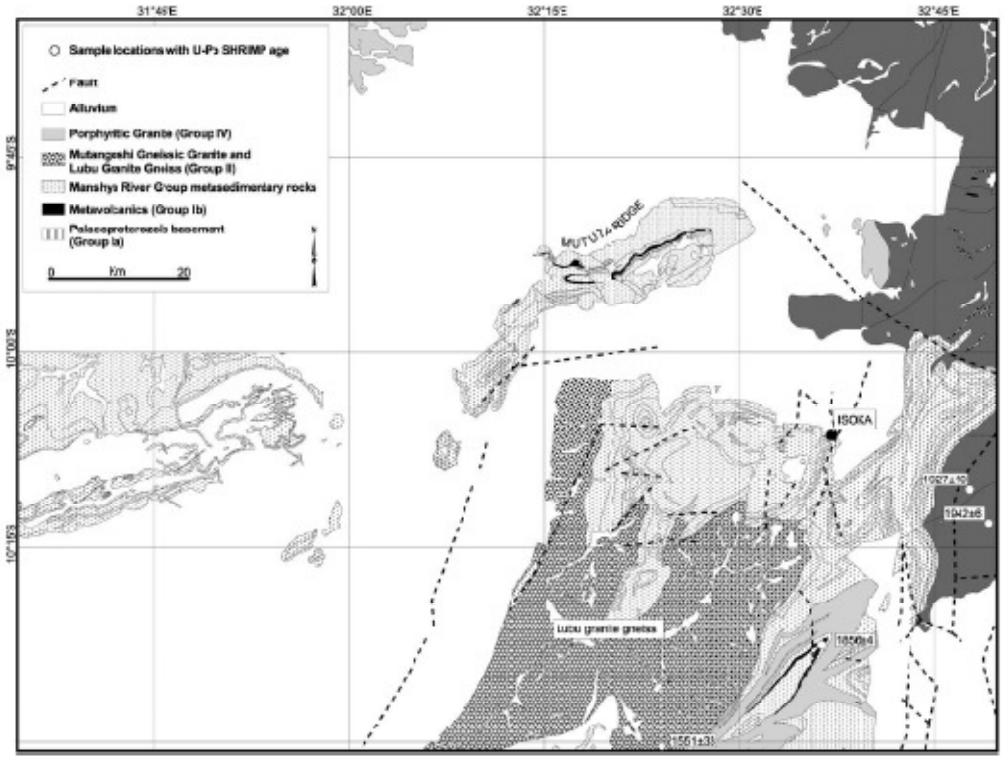

Fig. 10. Simplified geological map of the region around Isoka, based on published 1:100,000 scale geological maps, includes Makole, Mulilansolo Mission, and Mututa Hills map sheets, and parts of Isoka and Kalungu map sheets (Daly, 1994b,c; Van Tuijl and Verhoog, 1995)

led Daly and Unrug (1982) to suggest that these rocks represent reworked Mporokoso Group sedimentary rocks. This interpretation is supported by palaeocurrent directions indicating a sediment source to the northwest and west (present-day coordinates) (Andersen and Unrug, 1984). The lowermost part of the metasedimentary succession north of Isoka was previously termed the Mitoba River Group (Daly and Unrug, 1982) based on its predominant fluvial character as opposed to the shallow marine character typical for the Manshya River Group further south. Based on similar fluvial character, the Kasama Formation had been correlated with the Mitoba River Group (Daly and Unrug, 1982), and by inference with the lower part of the Manshya River Group (Daly, 1994a,b,c). Our new data show that the Kasama Formation is much younger than the lower Manshya River Group.

2.2.4. Manshya River Group

The Manshya River Group, first described by Marten (1968) from the Chalabesa Mission area (Fig. 4), comprises three pelite and two quartzite units in its type area along the Manshya River. These units can be followed ~120 km to the east where, in the Chimbwe syncline near Isoka, a marble unit occurs at the top, completing the stratigraphic succession. The continuous sequence exposed in the Chimbwe syncline begins with 1600 m of poorly exposed metapelites of the Lower Pelite Formation, comprising phyllite and slate. This basal unit passes higher up into the 1600-m-thick Mukonkoto Quartzite Formation, consisting of a lower massive quartzite member, followed by a poorly sorted coarse quartzite with detrital muscovite, and finally a well-sorted, medium-grained, pure quartzite. This is followed by the Mukonkoto Pelite Formation, which is poorly exposed and consists of phyllites and slates. The overlying Nkwale Quartzite Formation is characterised by a coarsening upward quartzite pelite package, grading up into an extensively cross-bedded, fine- to medium-grained pinkish quartzite, which is poorly sorted towards the top and grades into an impure quartzite. An interbedded pelite–quartzite succession overlies the impure quartzite. In the Chimbwe syncline, a thin marble occurs at the top of the sequence (Daly, 1995). Some

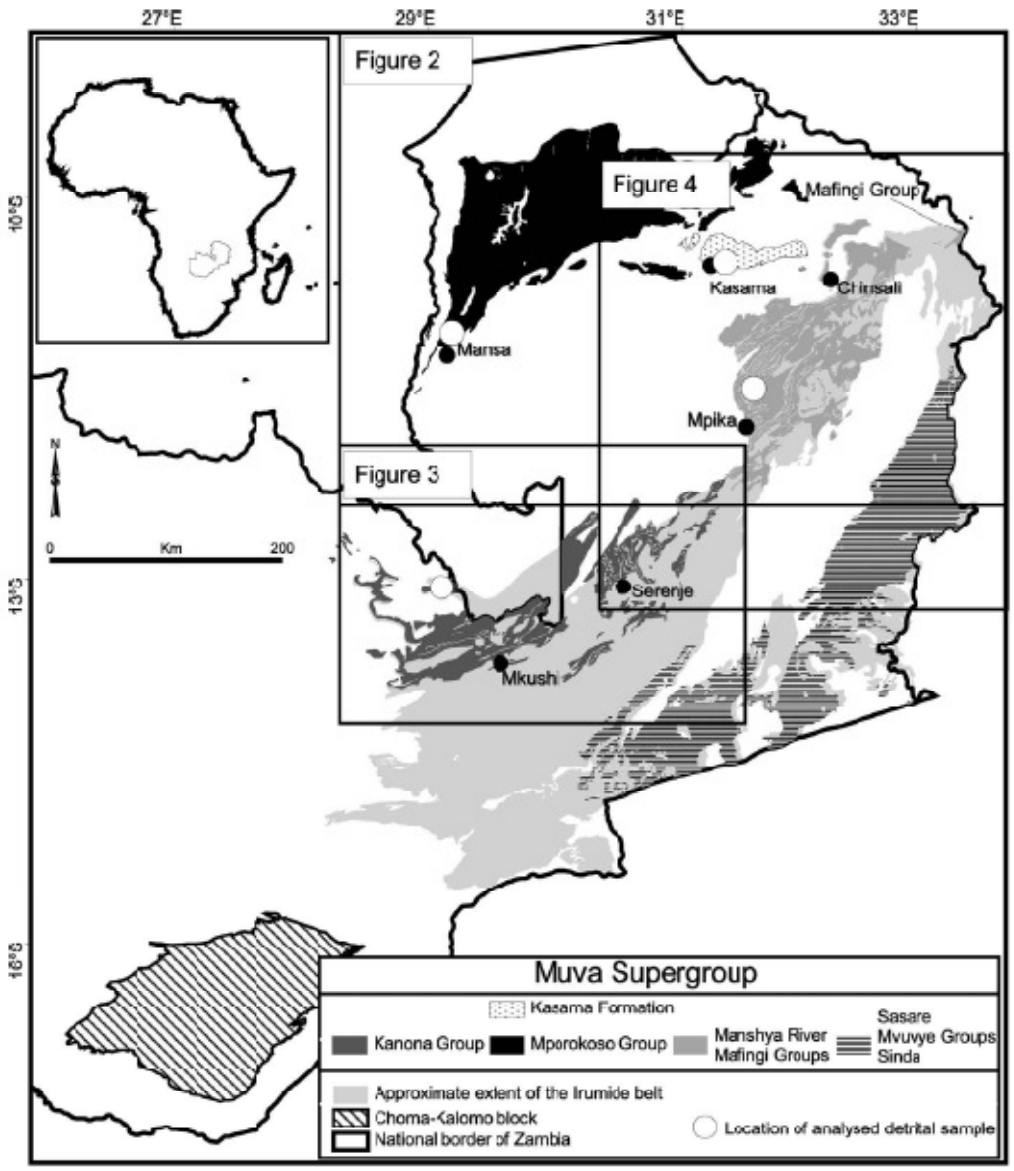

Fig. 11. Overview of the Palaeoproterozoic–Mesoproterozoic metasedimentary successions of Zambia. The boxes show the area of the detailed maps in Figs. 2-4.

80 km to the southwest, Ayres (1974) described stromatolites within the Manshya River Group in the Shiwa N'gandu area.

2.3.5. Kanona Group

The Kanona Group was redefined by De Waele and Mapani (2002) to comprise the deformed metasedimentary

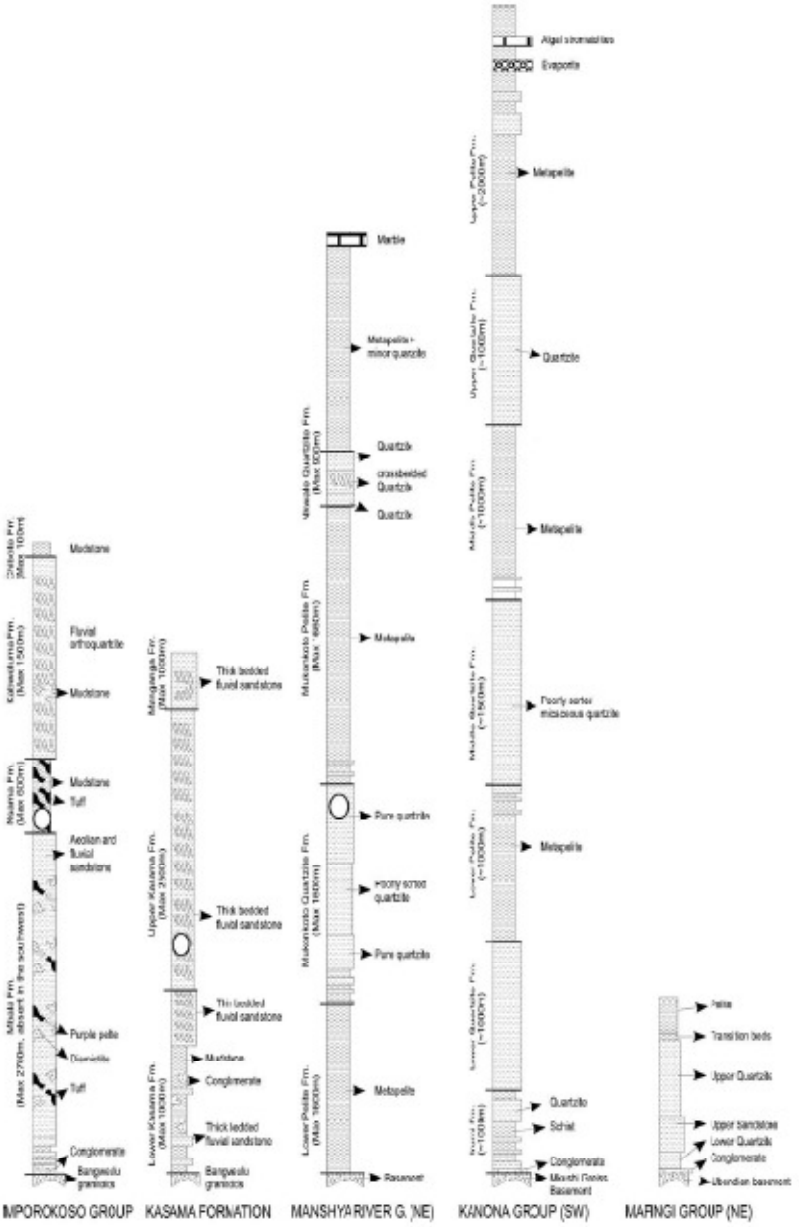

Fig. 12. Simplified lithostratigraphic columns for the Mporokoso Group, Kasama Formation, Manshya River Group, Kanona Group and Mafingi Group. The stratigraphy of the Mporokoso Group is adapted from Daly and Unrug (1982), the Kasama Formation from Unrug (1982), the Manshya River and Kanona Groups from Daly and Unrug (1982) and De Waele and Mapani (2002), and the Mafingi Group from Fitches (1971). The circles indicate the stratigraphic position of the samples analysed for detrital provenance.

sequences in the southwestern Irumide belt, and include a strongly tectonised basal part, consisting of mylonitic schist with subordinate quartzite units, called the Irumi Formation. The Irumi Formation is interpreted to include both tectonised basement lithologies and high-grade metasedimentary rocks at the thrust contact between the plutono-volcanic basement and supracrustal sedimentary and volcanic rocks. The metapelites are garnet–andalusite, garnet–biotite or kyanite schists, while the quartzite units include ferruginous muscovite quartzite, locally containing kyanite. No continuous sedimentary succession can be reconstructed in the southwestern Irumide belt, making the construction of a stratigraphic succession very difficult due to thrust duplication. Nevertheless, fragmentary successions documented at several places in the belt allow some reliable correlations and the reconstruction of a synthetic stratigraphic succession. The Kanona Group starts with a coarse quartzite with local conglomeratic layers. The quartzite shows current bedding and large-scale cross-bedding and is interbedded with ferruginous schist. The sequence grades into a flaggy metasiltstone, with slate and phyllite, which passes up into a micaceous, sugary quartzite member with minor pelitic schist. A second pelite unit consisting of slate and phyllite grades into a prominent quartzite sequence. This quartzite is recrystallised and pure, and practically no primary structure is preserved. A poorly exposed pelitic unit overlies the quartzite, and gradually coarsens upwards into a single or double quartzite horizon, in which ripple marks and small-scale cross-bedding are common. The uppermost part of the Kanona Group consists of a poorly exposed metasiltstone unit. Kerr (1975) and Smith and Kerr (1975) described localised evaporites and carbonates including algal stromatolites in the Fiwila Mission and Ndabala map sheets, which may correlate with those described at the top of the Manshya River Group (Ayres, 1974; Daly, 1986, 1995).

2.3.6. *Mafingi Group*

In northeast Zambia and northern Malawi, the Mafingi Group of Fitches (1971) rests unconformably on the Palaeoproterozoic Ubendian granulites and gneisses (Figs. 4 and 11). According to Fitches (1971) the group was first deformed during the Irumide orogeny, and can be tentatively correlated with the Manshya River Group. The Mafingi Group consists of quartzites that grade upwards into a metapelite unit. The quartzites are subdivided into four different formations. The basal siliciclastic (conglomerate and coarse sandstone) formation unconformably overlies granulites and consists mainly of a ~20-m-thick conglomeratic unit that contains clasts of the underlying lithologies. The Lower Quartzite Formation overlying the conglomerate has a maximum thickness of 210 m and is made up of a pure white quartzite. Ripple marks, trough cross-bedding and reverse and normal graded bedding are the main sedimentary features preserved. The Lower Quartzite Formation passes upwards into the 230-m-thick Upper Coarse Sandstone Formation. This poorly sorted sandstone contains conglomeratic and pelitic intercalations. Primary sedimentary features include herringbone cross-beds and graded bedding. Upwards, the sequence grades into the Upper Quartzite Formation, which forms a ~900-m-thick package of medium-grained mature sandstones, containing substantial amounts of detrital muscovite. Sedimentary features include planar cross-beds and large-scale herringbone structures that give a bimodal current direction between 0–40° and 160–200° (Fitches, 1971), inferred to reflect shallow marine, tidal conditions and/or beach deposits. This interpretation led Fitches (1971) to suggest a palaeo-shoreline oriented east–west during the deposition of the Upper Quartzite Formation.

2.3.7. *Mvuvye, Sinda and Sasare Groups*

Between the Karoo Luangwa graben and the Zambia–Mozambique border to the south, and the Zambia–Malawi border to the east, metasedimentary rocks of the Mvuvye, Sinda and Sasare Groups occur. These sedimentary successions comprise quartzites, graphitic schists, calc-silicates, marbles and volcanic rocks. The sequence records polyphase deformation, obliterating primary sedimentary structures, which along with the exposure gap across the Karoo graben, hampers direct correlations with the Muva sedimentary sequences to the north and northwest. Nevertheless, a tentative correlation was proposed by Daly (1986) and Johns et al. (1989) based on lithological similarities. Haslam et al. (1986) reported a Rb–Sr whole-rock date of 596 ± 10 Ma ($(^{87}Sr/^{86}Sr)_i = 0.71144 \pm 0.00085$) for the Sasare Group volcanic rocks (Fig. 5, Table 1, no. 1), and interpreted this date to record a metamorphic event soon after the extrusion of the lavas. If this interpretation were correct, the Sasare Group and its correlatives would belong to the Neoproterozoic sequences of the Zambezi belt and would thus not be part of the Muva Supergroup and the Irumide belt. However, little weight should be given to the Rb–Sr whole-rock date without supporting evidence, and more geochronological work is needed to resolve the issue satisfactorily. Johns et al. (1989) attempted to correlate the various metasedimentary units described in eastern Zambia, and distinguished three distinct successions: (1) the Basement Complex Supergroup comprising paragneisses and marbles; (2) the Chitundula Schist and Quartzite Formation comprising quartzites and metapelites and equated to the Manshya River Group (as they are affected by Irumide tectonism); (3) the Mwami Formation comprising pelites, psammites and metaconglomerates, unaffected by the Irumide orogeny. In the interpretation of Johns et al. (1989) the marbles, previously correlated to the Manshya River Group by Daly (1986), belong to an older, pre-Muva succession. Recent investigations in eastern Zambia (Mapani et al., 2001) have shown that the region to the southeast of the Irumide belt consists of a series of tectonically juxtaposed terranes, explaining the difficulties in correlating the various metasedimentary sequences. Unravelling the different sedimentary successions in eastern Zambia awaits further work.

2.3.8. Age of the Muva Supergroup

The Muva Supergroup is underlain by widespread volcanic units in the Bangweulu block, where rhyolitic ignimbrites occur beneath the Mporokoso Group. These ignimbrites yielded Rb–Sr and U–Pb zircon igneous crystallisation ages of ca. 1.86–1.82 Ga. Within the Irumide belt, occurrences of metavolcanic units within the Manshya River Group in the northeastern Irumide belt include the Luswa and Kachinga metarhyolitic tuffs that yielded SHRIMP U–Pb zircon crystallisation ages of 1879 ± 13 and 1856 ± 4 Ma respectively (De Waele et al., 2003a,b; De Wade and Fitzsimons, submitted for publication, Figs. 9 and 10, Table 1, nos. 77 and 67 respectively). Both rhyolitic tuffs were interpreted as waterlain volcaniclastic rocks (Daly, 1995; Sykes, 1995), whereas pillow lavas described in the Ibangwe Group of the Katibunga Mission area, which yielded a SHRIMP zircon U–Pb crystallisation age of 1871 ± 24 Ma (Fig. 8, Table 1, no. 73), indicate subaqueous extrusion (Mosley, 1979; Mosley and Marten, 1979). The similar ages for rhyolitic units in the Manshya River Group and immediately below the Mporokoso Group (1868 ± 7 and 1860 ± 13 Ma, Table 1, nos. 68 and 72) support the proposal that the two groups are coeval.

SHRIMP U–Pb dates on detrital zircon grains from prominent quartzites from the Mporokoso Group, Manshya River Group and Kasama Formation (Fig. 11) were analysed by De Waele and Fitzsimons (submitted for publication), and detrital age data for a quartzite from the Kanona Group near Mufulira (Fig. 5) was presented by Rainaud et al. (2003). Quartzite collected from the Mufulira mine area (sample MVQ1, Fig. 13a) in the Lufilian Arc and representing the southwestern continuation of the quartzites documented in the Irumide belt yielded prominent age populations of 3.02 Ga (8%), 2.70–2.40 Ga (23%), 2.39 Ga (6%), 2.30–2.12 Ga (39%) and 2.10–1.94 Ga (22%) (Rainaud et al., 2003), with the oldest and youngest grains at 3180 ± 12 Ma and 1941 ± 40 Ma respectively (Fig. 13a). Within the Manshya River Group, the Chembewesu Quartzite (sample IL14, Fig. 13b), southwest of Chinsali (Fig. 9) shows 47% of grains between 2.04 and 2.00 Ga, with the oldest and youngest concordant grains yielding 3011 ± 16 and 1882 ± 30 Ma respectively (Fig. 13b, De Waele and Fitzsimons, submitted for publication). In contrast, the Mwela Quartzite from the Kasama Formation (sample KAS, Fig. 13c) yielded a single detrital zircon of 1434 ± 13 Ma (96% concordant), which indicates that it is a younger sedimentary sequence (Fig. 13c, De Waele and Fitzsimons, submitted for publication). Ninety percent of the population of zircons from the Mwela quartzite of the Kasama Formation have an age between

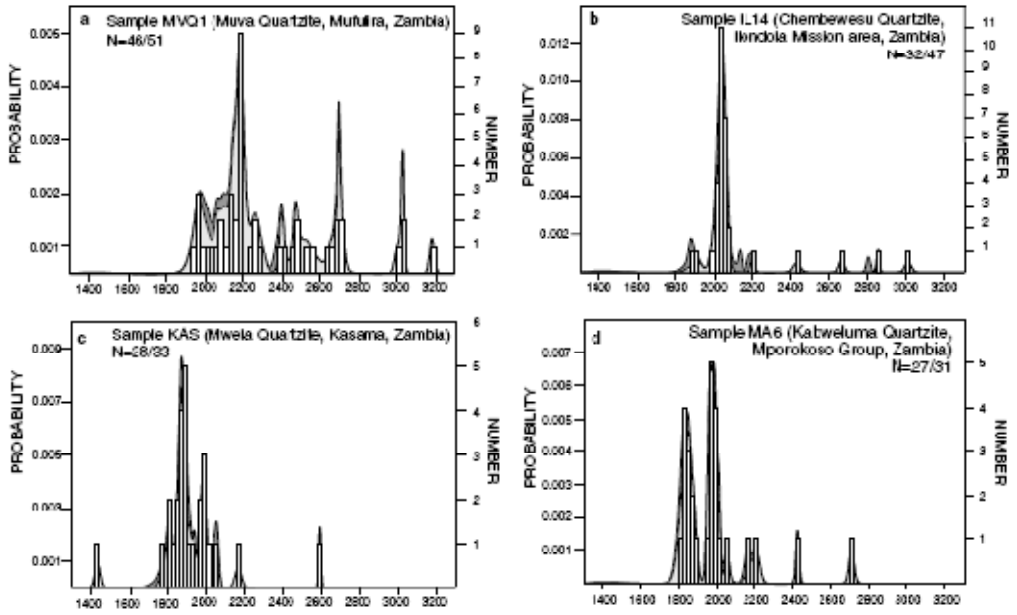

Fig. 13. Probability density distribution of SHRIMP U–Pb dates for concordant detrital zircon grains from the Chembewesu Quartzite (Manshya River Group), Mwela Quartzite (Kasama Formation), Mansa Quartzite (Mporokoso Group) and Mufulira Quartzite (Kanona Group). Data for the Mufulira Quartzite are after Rainaud et al. (2002). The location of the samples is indicated in Fig. 11, while their approximate stratigraphic position is indicated in Fig. 12.

1900 and 2050 Ma, with minor contribution of older populations at 2168 ± 17 Ma and 2593 ± 5 Ma. The detrital pattern of the Kasama Formation is consistent with its derivation from the Mporokoso Group to the northwest, as previously suggested by Andersen and Unrug (1984). A sample taken from the base of the Kabweluma Formation of the Mporokoso Group near Mansa (sample MA6, Fig. 13d) displays two equally represented populations, making up 80% of the total analyses (Fig. 13d). Zircon morphology suggests that both age populations have proximal as well as distal sources. Forty percent of the detrital zircons range in age from 1800 to 1900 Ma, while 40% range from 1950 to 2050 Ma. These two populations are clearly distinguishable, with a prominent trough between 1900 and 1950 Ma. The oldest concordant zircon has a $^{207}Pb/^{206}Pb$ age 2710 ± 13 Ma, while the youngest analysis provides a maximum age of deposition of the Kabweluma Formation at 1824 ± 19 Ma (Fig 13d, De Waele and Fitzsimons, submitted for publication). The age data indicate broad similarities of detrital zircons between the

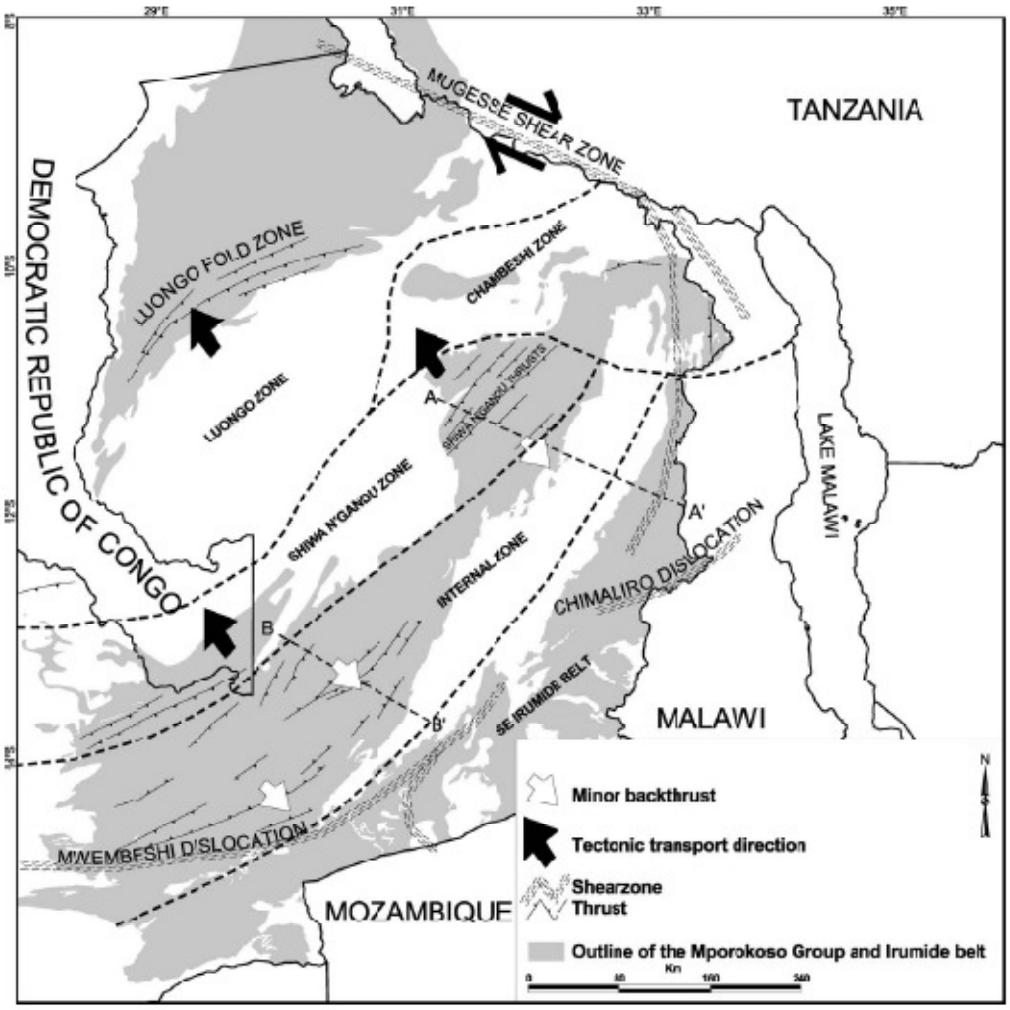

Fig. 14. Simplified structural map of the Irumide belt showing the structural zones recognised by Daly (1986) and discussed in the text. The positions of the cross-sections shown in Fig. 15 are indicated with dashed lines.

Chembewesu and Mufulira Quartzite of the Irumide belt and quartzite of the Kabweluma Formation (Mporokoso Group) near Mansa and are consistent with the emplacement ages of volcanic rocks underlying or interstratified with the sedimentary rocks in the Mporokoso and Manshya River Groups. Granitoids (1.65–1.55 Ga) intrude the Manshya River and Kanona Group sedimentary rocks and thus set their minimum depositional age. A younger zircon within the Kasama Formation indicates that sedimentation on the Bangweulu block continued after the 1.65–1.55 Ga magmatic event.

3. Structure

3.1. Introduction

The earliest structural investigations established the northeast structural grain of the Irumide belt (Ackermann, 1950). Extensive structural work by Daly (1986) recognised three separate structural zones, named Luongo, Chambeshi and Shiwa N'gandu zones. They are characterised by an increase of deformation intensity from the northwest (foreland zone) to the southeast (internal zone). The internal zone hosts the late Mesoproterozoic Irumide granitoids, intruding extensive pre-Mesoproterozoic basement units in the southwestern Irumide belt interpreted as a "pop-up" structure by Daly (1986). Daly (1986) described the Irumide belt and its foreland in terms of a northwest-verging fold and thrust belt and indicated that thrust displacement in the belt was accommodated along the Mugesse transcurrent shear zone within the Ubendian belt to the northeast (Fig. 2). This shear zone forms the northeastern boundary of the Irumide belt. Minor southeast-verging structures throughout the belt, especially to the southwest, were interpreted as back-thrusts related to the major northwest-directed thrusts. A brief description of the structures marking the Irumide belt is given below, from north to south: Luongo Fold Zone, Irumide belt s.s. and southeastern Irumide belt (Southern Irumide belt of Johnson et al., 2005; Fig. 14).

3.2. Luongo Fold Zone

In the Luongo Zone on the Bangweulu block, Daly (1986) identified a series of major basal shear zones below the Mporokoso Group sedimentary package and collectively called them the Bangweulu thrust. The Mporokoso Group sedimentary rocks overlying the ~1.85 Ga plutono-volcanic complex, define a major arcuate structure, strongly folded and structurally thrust on sub-horizontal strata to the north and west. Tectonic transport along the Bangweulu thrust is towards the northwest. K–Ar biotite dates between 1050 ± 31 and 991 ± 30 Ma for Palaeoproterozoic basement lithologies at or near the Bangweulu thrust, support a linkage between this thrust and the Irumide deformation to the south and southeast (Daly, 1986). Ca. 11 km shortening was calculated in the Mporokoso Group near Mansa (Daly, 1986).

3.3. Irumide belt s.s.

In the Irumide belt s.s., two episodes of deformation affected the rocks of the Manshya River and Kanona Groups (Daly, 1986). The earliest event (D_1) developed open F_1 folds with upright, northeast- to north–northeast-trending axial planes. Doubly plunging F_1 fold axes indicate a D_2 refolding event. A strong L_2 lineation, defined by sillimanite laths in metapelites, is well developed in the southwestern Irumide belt and is parallel to F_2 fold axes trending 25° → 050°. In the northeastern Irumide, fold axes related to D_2 trend north–northeast and the L_2 lineation plunges 75° → 235°. The relations between S_0 and S_1 in the northwestern Irumide are clear (low-grade metamorphism), but further southeast where the metamorphic grade increases, S_1 and S_2 fabrics become dominant. Contractional deformation in the Irumide belt induced northwesterly thrusting onto the Bangweulu block (Fig. 14). Up to 60 km of shortening is inferred to have occurred in the Manshya River Group in the northeast of the Irumide belt (Shiwa N'gandu thrusts, Fig. 14). Thrusts within the supracrustal sequence and ductile deformation at the basement-cover contact in the southwestern Irumide, near Mkushi, suggest that the Kanona Group was detached from its basement, while shallow plunging lineations throughout the Irumide belt confirm a northwest-directed tectonic transport. Minor back-thrusts are recognised, especially in the southwestern Irumide belt, producing a doubly-vergent character. The thrust interface in the southwestern Irumide is characterised by strong mylonitisation of metapelites and quartzites at the base of the Kanona Group. Fig. 15a shows two schematic sections across the Irumide belt in the northeast and southwest respectively (approximate locations of these sections are shown in Fig. 14).

3.4. Southeastern Irumide belt

Johns et al. (1989) recognised five deformation events in eastern Zambia, the two ascribed to the Irumide orogeny recording northwesterly tectonic vergence. However only three of these five deformation events can be correlated on a regional scale, one related to the Irumide deformation, and two to Pan African events. Mapani et al. (2001) proposed a tentative terrane subdivision of the southeastern Irumide belt, and suggested that eastern Zambia is underlain by a series of tectonic terrane stacks, including the parautochthonous Serenje, Luangwa and Nyimba terranes, which they regard as part of the Irumide Orogen (the region is referred to as the Southern Irumide Belt by Johnson et al. (2005)). The tectonic vergence in these terranes is also to the northwest. Daly (1986) linked the Mesoproterozoic deformation events in the Lurio belt of northern Mozambique to the structural development of the Irumide belt and postulated the existence of a pre-Mesoproterozoic microcraton (the Niassa craton) in southern Malawi, to explain the variation of structural vergence along a section running from

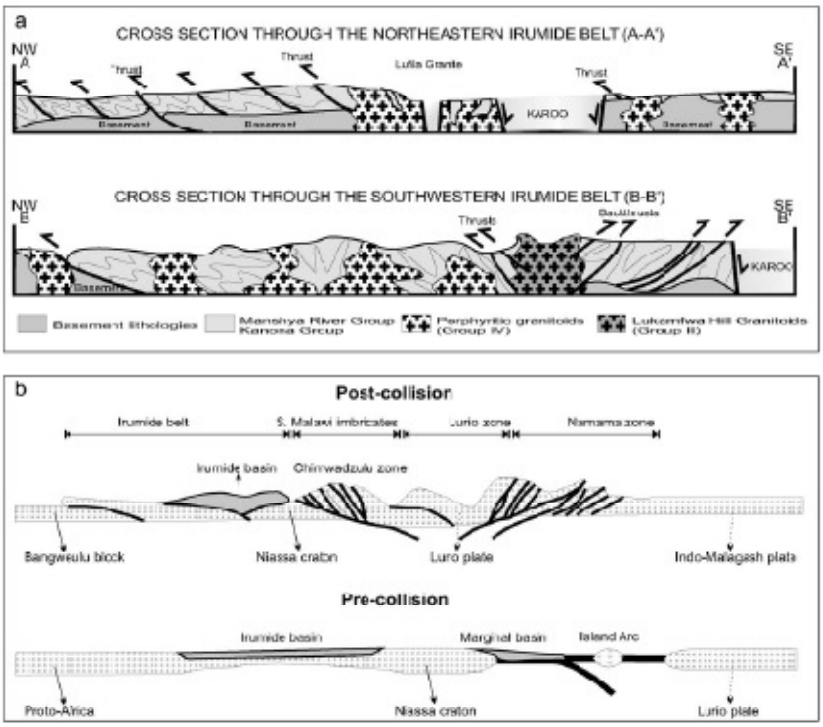

Fig. 15. Schematic cross-sections through the Irumide belt; (a) northeastern and southwestern Irumide belt (refer to Fig. 14 for locations); (b) regional cross-section through the Irumide belt, southeastern Irumide belt, southern Malawi and the Lurio belt (after Daly, 1986), showing pre- and post-collisional situation (see Fig. 1 for location).

the Irumide belt, across southeastern Zambia, southern Malawi and into northern Mozambique (Fig. 15b). More work is needed in the southeastern Irumide and adjacent Malawi and in northwestern Mozambique, to unravel this strongly overprinted and complex terrane.

4. Metamorphism

The general distribution of metamorphic facies in the Irumide belt is given in Ramsay and Ridgway (1977) and Ridgway and Ramsay (1986). The Irumide belt lies entirely in a northeast oriented amphibolite–greenschist grade metamorphic zone of the above authors (Fig. 16). Two metamorphic episodes (M_1 and M_2) are correlated with the S_1 and S_2 fabrics that developed during D_1 and D_2 respectively, with the regional structural grain of the belt developed during D_2. The Irumide belt is characterised by an increase of metamorphic grade, from sub-greenschist to greenschist facies in the foreland to the northwest, to amphibolite facies and localised granulite facies in the internal zone of the belt to the southeast. The metamorphic assemblages mark low-grade greenschist facies, with chlorite + muscovite + albite ± epidote, in the Mporokoso Group and are linked to the main thrusting episode, D_2. The rocks of the Manshya River and Kanona Groups increase in metamorphic grade from greenschist in the northwest to amphibolite facies in the southeast. The abundance of kyanite and sillimanite indicates medium-pressure/medium-temperature (Barrovian type) conditions. A preliminary study of metamorphism in the Serenje area (Mapani and Moore, 1995; Mapani, 1999), led to the identification of the following metamorphic zones, from northwest to southeast: biotite → garnet → staurolite → kyanite → sillimanite. Sillimanite + cordierite + garnet assemblages are common in migmatites and paragneisses in the far southeastern corner of the Serenje area (Fig. 3). Mapani and Moore (1995) and Mapani (1999) also report the coexistence of sillimanite and kyanite in recrystallised quartzite, and textural relations in metapelites indicating staurolite + gedrite + kyanite (M_1) being replaced by sillimanite + cordierite + gedrite + hornblende (M_2), followed by the growth of kyanite replacing sillimanite + cordierite

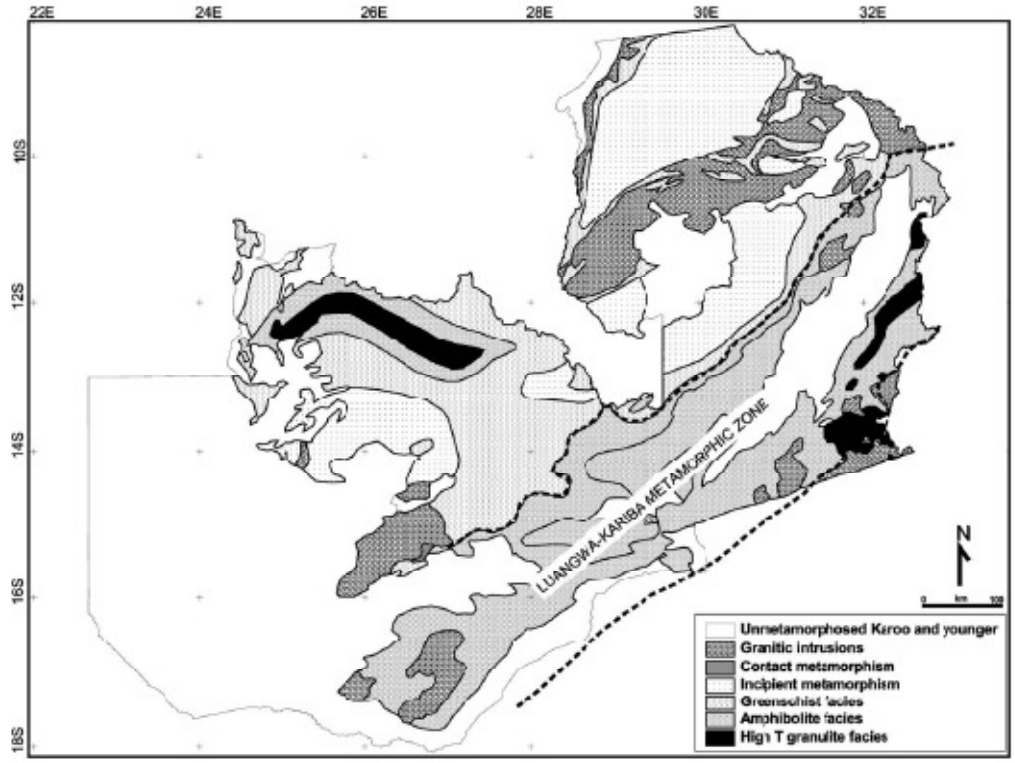

Fig. 16. Simplified metamorphic map of Zambia (after Ridgway and Ramsay, 1986).

along the S_2 fabric. In the Serenje and Kanona areas (Fig. 3), M_1 is generally obliterated. However, in the Mkushi and Ndabala areas (Fig. 3), Stillman (1965) records M_1 as biotite + garnet + quartz + muscovite and M_2 as muscovite + kyanite + quartz + andesine. In the Kanona area (Fig. 3), Vrána (1972) reports viridine $(Al,Mn,Fe)_2SiO_5$, the manganese variety of andalusite, to be intimately associated with gahnite ($ZnAl_2O_4$), the zinc spinel, along the S_2 fabric. Viridine in the M_2 assemblage likely records a late D_2 decrease of pressure. These textural relations indicate that the metamorphic evolution in the southwestern Irumide belt was quite complex.

In the northeastern Irumide, the more feldspathic lithologies are poor indicators of metamorphic grades. The metapelitic units commonly contain the assemblage biotite ± garnet + muscovite or staurolite ± garnet + biotite indicative of medium pressure/medium temperature (Barrovian type) conditions.

Available data indicate a clockwise *P–T–t* path during the syn-kinematic M_2 prograde Irumide metamorphism (Mapani and Moore, 1995; Mapani, 1999). This clockwise *P–T–t* path marks the crustal thickening stage of the orogeny, which ended with exhumation closely followed by a reheating episode coinciding with the widespread emplacement of granite bodies recording igneous crystallisation ages similar to the age of metamorphic rims of zircons in gneisses and migmatites (see below).

Granulite facies rocks are rare in the Irumide belt, and are clinopyroxene–orthopyroxene-bearing paragneisses, coexisting with sillimanite-bearing gneisses at the margins of batholiths (Daly, 1986) in northeastern Zambia. These assemblages do not record regional metamorphic grades as they were linked to contact metamorphism (Sykes, 1995) with granulite facies assemblages rarely extending over more than a few tens of metres.

The timing of M_2 peak metamorphism in the southwestern Irumide belt is constrained by SHRIMP U–Pb zircon dates from low-Th/U metamorphic rims on zircons from migmatitic gneisses in the Serenje area, which range between 1021 ± 16 and 1018 ± 5 Ma (samples SER 6-6 and SER 6-7 in Fig. 7, Table 1, nos. 13 and 16, De Waele et al., 2003c). Similar metamorphic zircon rims from a gneiss in the northeastern Irumide belt near Chinsali (Fig. 9, Table 1, no. 12) yielded a SHRIMP U–Pb zircon

date of 1004 ± 16 Ma (De Waele, 2005). In contrast, metamorphic rims on zircon from an Archaean (2608 ± 14 Ma) diorite-granodiorite gneiss near Luangwa, south of Serenje (Fig. 5, Table 1, no. 33), yielded a LA–ICP–MS date of 1043 ± 19 Ma (Cox et al., 2002). This gneiss represents an Archaean basement, reworked in the Irumide belt, and the metamorphic zircon rims date peak Irumide metamorphism. A U–Pb monazite date of 1046 ± 3 Ma, interpreted to date peak metamorphism in granulite gneisses near Chipata (Fig. 5, Table 1, no. 34, Schenk and Appel, 2001), indicates that peak metamorphism is ~30 Ma older in the southeastern Irumide belt than in the Irumide belt s.s. Peak metamorphism is linked to crustal thickening between ~1050 and 1020 Ma, as the metamorphic ages overlap the age-range of syn-kinematic Irumide granitoids (De Waele et al., 2003c).

5. Magmatism

Six distinct igneous events mark the evolution of the crustal section affected by the Mesoproterozoic Irumide deformation. Rocks emplaced during the first igneous event include Archaean granite–tonalite gneisses emplaced between 2.73 and 2.61 Ga (Fig. 5, Table 1, nos. 108 and 109). Neoarchaean rocks are known only at two localities, one north of Kapiri Mposhi, and one east of Luangwa (Fig. 5). The second igneous event is widespread and include two closely-spaced, sub-suites (termed Group Ia and Group Ib) made of variably deformed plutonic and plutono-volcanic bodies emplaced between ~2.05–1.93 Ga and 1.88–1.85 Ga respectively. The Palaeoproterozoic magmatic rocks within and underlying the Irumide belt are outside the scope of this paper and will not be discussed further.

The third igneous event (termed Group II) includes biotite orthogneisses that yielded zircon igneous crystallisation ages between ~1.66 and 1.55 Ga. The fourth igneous event (termed Group III), is represented by a nepheline syenite and a biotite metasonalite emplaced at ~1.36–1.33 Ga in the extreme northeast of the Irumide belt. Group II and Group III igneous rocks pre-date the Irumide orogeny, but they are briefly discussed in this paper because they extend into the Mesoproterozoic. The youngest igneous event is recorded by large bodies of peraluminous, K-feldspar-phyric to megacrystic biotite granites, foliated porphyritic biotite granites and garnetiferous two-mica granites (Group IV) that yielded zircon igneous crystallisation ages of 1.05–0.95 Ga, coeval with and post-dating the peak of the Irumide orogeny. Group IV igneous rocks represent the main magmatic episode directly related to the Irumide orogeny.

An attempt was made by Tembo et al. (2002) to characterise the various granitoids of the Irumide belt. Tembo et al. (2002) reported very similar geochemical characteristics for all granite suites, which were subdivided into pre-syn- and post-tectonic granitoids. According to Tembo et al. (2002), all suites are characterised by high potassium content, strong enrichment in LILE and HFSE and low TiO_2 content, leading to the interpretation that all granitoids had incorporated significant amount of crustal melt with calc-alkaline affinity. We here present new geochemical data on selected samples of the granitic suites, including major elements (ICP–OES) and trace elements (ICP–MS). These data are summarised in Tables 2, 3 and 4a–d.

5.1. Group II pre-Irumide granitoids (1.65–1.55 Ga)

Group II granitoids exposed in the northeastern Irumide belt between Mpika and Chinsali (Figs. 8–10), are gneissic

Table 2
Representative major and trace element geochemistry of Group II granitoids (1.65–1.55 Ga) in the Irumide belt

	LW10	SER62	ND2	SR12	SR6	SR7
SiO_2	70.24	72.55	71.92	77.30	74.31	65.38
Al_2O_3	14.05	12.39	13.83	12.54	12.67	17.03
Fe_2O_3	2.79	4.04	2.76	2.04	2.61	4.10
MnO	0.03	0.09	–	–	–	–
MgO	0.40	0.22	0.24	0.16	0.05	0.28
CaO	0.83	1.17	1.31	0.73	0.87	2.00
Na_2O	2.18	2.70	3.52	2.21	2.69	3.49
K_2O	6.53	6.02	4.69	5.26	4.82	6.38
TiO_2	0.58	0.42	0.30	0.33	0.30	0.51
P_2O_5	0.39	0.05	0.09	0.06	0.05	0.08
LOI	0.56	–	0.00	0.01	0.00	0.01
Total	98.75	99.65	97.66	100.62	98.37	99.23
Rb	292	209	172	329	310	267
Cs	–	0.80	1.78	1.82	1.19	0.77
Pb	44.1	30.0	18.8	40.0	45.7	55.5
Ba	1456	1125	1169	448	370	1375
Th	34.3	35.0	15.6	34.9	39.4	31.8
U	2.06	2.00	3.05	2.83	3.87	2.90
Nb	30.2	43.0	25.7	66.8	81.3	70.7
La	116	217	83	118	207	94
Ce	185	314	175	288	409	306
Sr	78	72	86	24	16	65
Pr	20.7	30.0	19.2	22.5	41.8	22.6
Nd	81	183	71	80	152	90
Zr	288	937	77	339	386	408
Sm	15.3	31.0	16.4	16.8	39.8	20.9
Eu	2.14	3.50	2.52	1.43	3.33	2.97
Gd	12.8	29.7	14.8	15.1	45.1	17.7
Tb	0.95	3.00	2.98	2.90	10.50	3.66
Dy	10.7	20.3	16.9	15.6	54.0	18.0
Y	64	83	96	89	311	101
Ho	1.82	3.70	2.86	2.87	10.47	3.21
Er	5.14	10.20	8.67	8.69	29.65	9.73
Tm	1.46	0.95	1.45	1.59	4.90	1.70
Yb	6.17	8.00	8.63	9.49	32.12	9.70
Lu	0.91	1.10	1.51	1.46	5.24	1.65
Zn	55	100	98	84	219	617
Cu	12.81	–	3.73	2.60	13.85	17.82
Ni	5.49	5.00	2.13	2.58	3.22	2.78
Cr	11.53	–	6.92	7.08	6.37	7.83
Co	45.3	19.0	40.9	10.3	6.8	15.9
Ga	16.7	23.0	24.8	19.5	21.2	28.9
Hf	8.16	18.00	2.32	10.40	12.61	10.99
Sn	5.78	4.00	2.81	6.26	7.56	9.60
Ta	3.59	9.50	1.73	2.24	2.06	2.21
W	38.8	176.0	25.4	11.4	7.2	14.4

Table 3
Representative major and trace element geochemistry of Group III plutonic rocks (Group III granitoids (Mivula syenite)) in the northeastern Irumide belt (data from Tembo, 1886)

	M13	M8	M4	M1	M23	M21	M7	M16	M2	M11	M3	M9	M M6	M10
SiO_2	50.28	51.11	53.35	53.87	54.05	54.35	54.62	55.12	55.24	55.43	51.05	52.87	53.45	53.63
Al_2O_3	19.52	24.86	20.86	23.7	23.07	21.18	21.64	21.26	21.38	21.13	19.66	19.95	21.12	20.2
Fe_2O_3	8.99	3.19	6.51	4.22	1.57	5.92	4.62	5.19	5.32	5.87	8.89	8.91	5.83	6.4
MnO	0.17	0.09	0.18	0.08	0.14	0.11	0.15	0.2	0.12	0.12	0.23	0.15	0.14	0.15
MgO	1	0.12	0.17	0.11	0.15	0.52	0.12	0.17	0.57	0.64	1.22	0.56	0.59	0.89
CaO	3.55	1.55	3.17	0.95	1.88	1.1	2.77	1.92	2.62	0.35	3.84	1.66	2.77	2.33
Na_2O	7.9	11.65	6.84	9.2	9.76	7.28	7.36	7.79	5.3	5.87	6.2	5.94	7.67	6.75
K_2O	7.62	7.12	8.25	7.46	7.52	8.42	8.23	7.87	8.43	9.4	7.14	8.86	7.53	8.44
TiO_2	0.9	0.29	0.58	0.36	0.3	1.06	0.43	0.48	0.92	1.15	1.52	1.04	0.74	1
P_2O_5	0.05	0.01	0.08	0.01	0.04	0.05	0.04	0.01	0.09	0.04	0.25	0.05	0.17	0.18
LOI	2.38	2.25	2.87	1.74	1.59	2.3	2.34	0.84	1.93	1.11	2.4	1.1	3.86	0.72
Total	102.36	102.24	102.86	101.73	100.07	102.29	102.32	100.85	101.92	101.11	102.40	101.09	103.87	100.69
Rb	283	210	184	210	236	145	222	271	135	195	184	345	229	231
Ba	3580	737	2210	966	517	4560	1920	309	6870	5080	4360	2370	2520	3540
Nb	35	68	72	66	91	91	114	107	106	143	207	131	178	136
La	2.00	12.00	20.00	6.00	50.0	29.0	36.0	19.00	23.00	2.00	19.00	7.00	28.00	10.00
Ce	5.00	34.0	49.0	21.00	97.0	51.0	66.0	39.0	43.0	10.00	38.0	22.00	58.0	34.0
Sr	1500	1630	1960	1570	1170	2190	2310	1120	2170	1450	796	1400	1830	1460
Nd	13.00	13.00	27.0	11.00	38.0	37.0	34.0	16.00	42.0	19.00	37.0	10.00	34.0	24.00
Zr	79	196	149	124	222	75	166	219	144	84	437	137	367	257
Y	3.80	6.80	10.00	4.70	17.00	10.00	12.00	10.00	11.00	3.80	15.00	6.90	13.00	9.70
Cr	3.00	3.00	4.00	4.00	5.00	3.00	30.00	3.00	3.00	3.00	25.00	5.00	18.00	4.70
Ga	29.0	23.00	16.00	21.00	23.00	21.00	17.00	23.00	23.00	23.00	25.00	24.00	20.00	24.00

and foliated granitoids, known as the Mutangoshi Gneissic Granite and Lubu Granite Gneiss. In the southwest, between Mpika and Mkushi (Fig. 6 and 7), Group II granitoids are known as the Lukamfwa Hill Granite Gneiss. Granitoids and orthogneisses of this group were previously poorly dated, but regarded to be related to initial stages of the Irumide orogeny in the northeast (Daly, 1986), or undated but presumed to pre-date Irumide tectonism in the southwest, where they were ascribed to the Palaeoproterozoic Mkushi Gneiss Complex (Stillman, 1965).

Group II granitoids form plutons of grey biotite gneiss, containing biotite (locally retrograded to chlorite) or biotite ± hornblende. Based on field relations indicating that they intrude the Muva Supergroup, and the strong north- to north–northeast-trending foliation, the orthogneiss complexes were assumed to be syn-kinematic intrusions with respect to the Irumide compressional deformation (Stillman, 1965; Smith, 1966; Page, 1973; Cordiner, 1977; De Waele and Mapani, 2002). Daly (1986) interpreted these orthogneisses as pre-kinematic intrusions, deformed together with the supracrustal metasedimentary sequence.

The Lukamfwa Hill Granite Gneiss in the southwestern part of the Irumide belt ranges from coarse phenocrystic varieties to finer grained phases. In the type locality of Lukamfwa Hill in the Serenje area, these rocks consist of coarse-grained, K-feldspar-phyric granite gneiss, with a strong northeast foliation defined by biotite that wraps stretched microcline phenocrysts, imparting an augen texture. The gneiss is intensely folded, with isoclinally folded quartz veins and axial planar S_1 biotite foliation defining a first deformational event. A crenulation of the biotite foliation along a northeast S_2 foliation defines a second deformation. The two deformational events are recorded in both the coarse- and fine-grained gneisses.

The Mutangoshi Gneissic Granite and its equivalents in the Chinsali area (Fig. 9) form large bodies of strongly foliated grey biotite orthogneiss, affected by east–west discrete shear zones. The rocks contain abundant biotite (locally retrogressed to chlorite) or biotite + hornblende. They show evidence of polyphase deformation, with a northeast–southwest gneissic fabric cut by steep east–west shear zones accompanied by C-S fabrics and steep lineations. Numerous melt veins intrude the gneiss and display ptygmatic folds along east–west axes. Daly (1986) interpreted the Mutangoshi Gneissic Granite as a pre-kinematic intrusion, deformed together with the supracrustal sequence. He pointed out that the deformed granitoids are closely associated with amphibolites and suggested that the two belong to a pre-kinematic extensional bimodal magmatic event. The Mutangoshi Gneissic Granite occurs together with a compositionally very similar suite of younger granites called the Chilubanama Granite (Daly, 1986), which belong to Group IV granitoids (see below).

The Musalango Gneiss in the Luswa River area, previously equated with the Mutangoshi Gneissic Granite (Daly, 1986; Sykes, 1995), yielded a SHRIMP U–Pb date of 1610 ± 26 Ma (Fig. 9, Table 1, no. 58, De Waele et al., 2003c). The Lubu Granite Gneiss, which was previously assigned to the Palaeoproterozoic Basement (Daly, 1995), yielded a SHRIMP U–Pb zircon date of 1551 ± 33 Ma (Fig. 9, Table 1, no. 57, De Waele et al., 2003c). In the southwestern part of the belt, the Lukamfwa Hill Granite

Table 4a
Representative major and trace element geochemistry of Group IV granitoids in the southwestern Irumide belt

	MH4	MH5	MH9C	MK2	MK7	ND1	ND5	SR5	SR9	MQG-1
SiO_2	74.58	74.20	70.67	76.53	73.21	71.56	64.65	73.56	69.95	74.55
Al_2O_3	12.41	14.46	16.17	13.39	14.64	14.49	14.44	14.75	14.90	13.09
Fe_2O_3	3.63	1.51	2.07	0.69	1.43	1.54	4.77	3.56	3.33	1.67
MnO	–	–	–	–	–	–	–	–	–	0.04
MgO	1.54	0.44	0.49	0.27	0.41	0.15	2.48	0.62	0.69	0.11
CaO	2.71	0.95	1.64	0.79	0.49	0.76	2.70	1.59	2.37	0.79
Na_2O	1.86	2.59	2.72	2.60	3.63	2.73	3.08	1.86	3.28	3.28
K_2O	1.89	3.86	4.60	4.52	5.18	7.59	5.87	5.08	4.25	6.13
TiO_2	0.53	0.27	0.46	0.11	0.27	0.22	0.82	0.77	0.64	0.13
P_2O_5	0.04	0.08	0.12	0.11	0.08	0.07	0.10	0.09	0.10	–
LOI	0.00	0.01	0.01	0.02	0.01	0.01	0.10	0.01	0.01	–
Total	99.19	98.36	98.94	99.01	99.33	99.11	98.92	101.89	99.51	99.79
Rb	269.8	194.7	222.7	254.3	280.3	329.3	361.0	259.4	155.7	210.0
Cs	3.7	6.2	2.1	3.7	1.1	1.3	5.9	2.1	2.7	2.4
Pb	36.4	34.8	32.6	30.9	17.0	42.9	25.1	44.7	19.5	45.0
Ba	1432.0	725.3	1346.5	331.3	721.4	776.5	4595.1	1551.4	966.9	207.0
Th	12.5	18.9	21.0	7.1	27.1	38.9	41.0	15.8	15.4	41.0
U	1.4	2.2	1.6	1.6	5.6	2.0	7.2	0.9	0.9	4.0
Nb	25.3	12.8	12.4	6.0	30.8	9.9	27.8	10.8	13.1	15.0
La	53.1	25.0	68.3	13.9	45.2	51.3	126.2	17.0	38.2	121.5
Ce	129.5	56.8	127.3	30.3	96.7	118.8	248.0	91.7	81.7	248.0
Sr	125.7	79.0	168.5	74.9	87.9	88.2	761.4	106.1	178.1	25.6
Pr	10.6	5.7	12.5	3.2	9.7	11.7	24.2	3.8	8.0	28.0
Nd	40.2	21.3	39.3	10.8	34.7	41.3	84.2	15.4	29.4	103.5
Zr	268.6	154.1	153.3	122.4	196.6	112.3	275.1	196.0	127.4	234.0
Sm	6.9	4.3	6.4	2.8	7.5	8.1	17.0	3.8	6.5	18.0
Eu	1.0	0.4	1.3	0.6	0.7	1.3	4.0	0.8	1.6	1.0
Gd	5.1	2.9	4.3	2.1	5.1	5.2	10.9	2.9	4.9	16.5
Tb	1.0	0.5	0.7	0.4	0.9	0.7	1.7	0.5	1.0	2.0
Dy	4.3	1.8	2.8	2.3	4.3	2.9	7.3	2.8	3.9	11.4
Y	21.5	6.5	13.8	15.9	20.7	10.7	41.0	12.4	19.3	48.0
Ho	0.7	0.2	0.3	0.4	0.7	0.4	1.0	0.4	0.7	2.1
Er	1.9	0.6	1.1	1.1	2.0	1.0	2.9	1.1	1.7	5.8
Tm	0.4	0.1	0.2	0.2	0.3	0.1	0.5	0.2	0.2	1.6
Yb	2.2	0.4	0.7	1.0	1.7	0.5	2.8	1.1	1.0	4.9
Lu	0.4	0.1	0.1	0.2	0.3	0.1	0.5	0.1	0.2	0.8
Zn	93.0	42.7	46.2	19.0	21.7	25.8	126.3	85.2	53.3	55.0
Cu	14.2	5.9	5.8	12.8	7.4	3.0	69.8	12.3	9.1	5.0
Ni	4.3	6.6	3.8	1.8	3.3	2.6	30.7	5.8	5.0	10.0
Cr	11.6	16.8	9.1	8.6	7.9	7.1	56.2	12.9	12.2	–
Co	16.1	10.4	13.0	12.7	73.5	22.9	39.0	27.5	31.5	19.0
Ga	23.8	15.4	18.1	10.3	19.9	20.0	24.5	21.8	17.4	23.0
Hf	6.8	4.3	3.4	2.2	5.6	3.5	5.6	4.9	3.6	8.0
Sn	2.3	1.3	0.7	1.9	2.1	0.8	1.8	1.0	1.3	3.0
Ta	0.7	0.6	0.6	0.7	4.7	1.3	1.2	0.6	2.2	9.0
W	8.5	6.5	5.2	10.1	56.1	16.9	12.4	13.8	30.7	184.0

Gneiss, yielded SHRIMP U–Pb zircon dates of 1664 ± 4, 1652 ± 6, 1639 ± 14 and 1627 ± 12 Ma (Figs. 6 and 7, Table 1, nos. 59–62, De Waele et al., 2003c).

Major element analyses of Group II granitoids (Table 2) show a uniform composition, with a relatively small range for most oxides ($SiO_2 = 69.38$–77.30%, $TiO_2 = 0.26$–0.58%, $Al_2O_3 = 11.91$–14.05%, total $Fe_2O_3 = 1.43$–4.10%, $MgO = 0.05$–0.40%, $Na_2O = 2.18$–3.52% and $K_2O = 4.18$–6.53%). In the Q–A–P normative classification diagram, these granitoids plot in the field for monzogranite (Fig. 17a). The distribution of the data in Fig. 17b shows that these rocks range from metaluminous to peraluminous, with peraluminous compositions dominating. Their alumina saturation index (ASI = molecular ratio $Al_2O_3/(CaO + Na_2O + K_2O)$) ranges from 0.80 to 1.18, and K_2O/Na_2O ratios range between 1.33 and 3.00, indicating that these are potassic granitoids (Fig. 17c).

Group II granitoids show a wide range for Rb (172–493 ppm), Ba (370–1456 ppm), Zr (77–637 ppm), Sr (16–86), Nb (26–81 ppm) and Y (24–311 ppm). In the diagram K versus Rb (Fig. 17d), these granitoids define evolution trends similar to the magmatic trends defined by granitoids not affected by significant post-magmatic "alteration" and are characterised by K/Rb ratios between

Table 4b
Representative major and trace element geochemistry of Group IV granitoids in the southern Irumide belt

	CC4	CC5	CC8	KK1	KN2A	KN4	KN5	KN7	KN8	KN8b
SiO_2	75.72	73.43	74.10	68.82	72.11	72.50	68.84	75.28	69.04	72.45
Al_2O_3	12.82	13.56	13.12	14.94	13.40	14.69	13.82	13.74	15.72	14.55
Fe_2O_3	1.66	4.12	2.04	3.74	2.46	1.61	5.24	1.33	2.57	2.68
MnO	–	–	–	–	–	–	–	–	–	–
MgO	0.29	0.70	0.48	0.55	0.25	0.40	1.51	0.28	0.84	0.87
CaO	0.98	2.41	1.62	2.65	1.80	1.24	2.96	0.89	1.57	1.70
Na_2O	2.75	2.95	2.84	2.08	2.63	2.81	2.64	2.71	2.37	2.63
K_2O	4.21	3.72	3.84	4.85	4.85	4.90	3.31	4.36	5.08	4.90
TiO_2	0.21	0.72	0.45	0.51	0.48	0.69	1.05	0.21	0.50	0.51
P_2O_5	0.08	0.15	0.06	0.14	0.11	0.23	0.10	0.11	0.14	0.16
LOI	0.01	0.00	0.01	0.01	0.00	0.01	0.00	0.01	0.01	0.01
Total	98.71	101.74	98.54	98.07	98.19	99.07	99.28	98.91	97.79	100.45
Rb	183.5	116.0	168.4	204.4	202.5	332.2	177.3	284.7	241.5	260.8
Cs	1.8	1.5	1.3	1.2	2.7	7.2	5.4	2.5	4.8	5.9
Pb	25.7	26.3	17.7	47.2	27.2	62.9	19.1	46.3	62.9	78.5
Ba	1032.2	1762.0	1099.0	1401.1	1642.5	1056.0	943.6	519.6	2853.7	3685.0
Th	15.4	5.0	20.1	34.6	12.8	30.1	12.4	32.8	22.9	23.2
U	2.6	1.4	2.7	1.0	1.5	2.7	3.3	2.5	1.2	2.0
Nb	16.9	12.9	10.6	25.1	19.5	24.6	5.1	18.6	20.0	19.7
La	55.1	29.8	75.6	83.6	47.6	48.5	44.0	32.1	169.5	154.7
Ce	111.7	73.2	153.7	192.5	117.1	117.0	107.7	88.6	177.9	152.8
Sr	114.6	194.3	171.2	161.2	131.4	150.9	118.0	104.6	549.5	566.8
Pr	11.1	7.3	14.6	17.1	10.3	10.3	9.6	6.9	29.9	28.7
Nd	36.5	27.6	50.6	62.1	37.6	35.5	35.6	24.0	102.1	105.8
Zr	188.5	84.7	126.4	127.1	116.7	212.3	63.6	206.5	124.0	167.2
Sm	7.0	5.9	10.1	11.8	8.4	6.5	7.9	4.9	19.9	18.7
Eu	0.9	1.6	1.4	2.1	2.1	0.9	1.5	0.6	3.6	3.3
Gd	5.1	4.6	7.1	9.3	7.6	3.4	6.1	3.1	12.4	12.0
Tb	0.8	0.8	1.3	1.5	1.2	0.5	1.1	0.5	1.9	1.8
Dy	3.6	4.2	6.3	6.7	6.6	2.0	5.4	1.7	7.3	7.4
Y	18.4	20.8	38.6	39.4	39.8	9.8	33.1	10.6	38.4	31.2
Ho	0.5	0.7	1.0	1.2	1.1	0.2	1.0	0.3	1.0	1.1
Er	1.3	2.0	3.2	3.2	3.6	0.7	2.8	0.7	2.7	2.8
Tm	0.2	0.3	0.6	0.5	0.4	0.1	0.5	0.1	0.3	0.4
Yb	0.8	1.8	3.9	3.0	2.8	0.8	3.0	0.7	1.6	1.9
Lu	0.2	0.3	0.6	0.4	0.5	0.1	0.5	0.1	0.2	0.2
Zn	42.3	95.5	50.3	79.5	59.6	56.9	79.1	46.9	55.3	59.5
Cu	3.2	12.9	6.5	14.0	5.5	3.7	14.8	2.6	7.5	8.6
Ni	3.0	4.4	3.5	3.9	2.8	4.2	10.7	3.7	10.8	11.0
Cr	9.9	12.0	12.0	7.0	8.8	9.1	24.9	7.7	22.1	24.2
Co	11.2	17.6	13.5	75.1	16.7	63.8	24.7	6.6	18.2	19.0
Ga	18.3	18.7	17.7	23.7	20.7	22.6	19.8	17.5	17.8	19.9
Hf	4.9	2.1	3.5	2.1	3.6	5.6	1.6	4.7	2.7	2.7
Sn	1.6	1.0	1.4	1.0	1.3	2.7	1.1	2.3	1.9	2.3
Ta	1.2	0.4	0.6	2.7	0.5	3.9	0.3	0.8	1.1	0.7
W	7.1	7.0	4.5	45.5	12.2	35.9	3.9	5.2	9.7	11.7

130 and 240; therefore, the alkali contents in these granitoids are likely to be close to the original compositions. The relationships between Rb, Y and Nb (Pearce et al., 1984; Pearce, 1996, Figs. 17e and f) suggest that these granitoids are either anorogenic within-plate granites or late to post-orogenic granitoids. However, strongly peraluminous compositions are not common in anorogenic settings (Sylvester, 1989; Pitcher, 1997), and where peraluminous granitoids were documented in anorogenic settings, they usually represent rocks affected by strong post-solidus hydrothermal alteration and are documented together with alkaline/peralkaline granitoids (Kinnaird and Bowden, 1991). We therefore interpret Group II granitoids as collision-related, rather than anorogenic granitoids.

The rare-earth element (REE) contents are 626–1611 times chondritic values (normalisation values after McDonough and Sun, 1995, Fig. 18a), except for Eu. La_N/Yb_N values fall in the range 4.4–18.4. The light REE (LREE) display a fractionated pattern (La_N/Sm_N: 2.8–4.8), whereas the heavy REE (HREE) are marked by nearly flat patterns (Gd_N/Yb_N: 1.1–3.0). All the REE patterns display a negative Eu anomaly (Eu/Eu*: 0.24–0.48; where Eu* is derived by linear interpolation between Sm and Gd). Multi-element patterns of Group II granitoids, normalised to primordial mantle, show negative anomalies

Table 4c
Representative major and trace element geochemistry of Group IV granitoids in the northern Irumide belt

	SH8	SH9	LW1	MTG1	MTG5
SiO_2	70.40	74.62	72.41	73.32	74.76
Al_2O_3	14.05	12.14	14.51	14.04	13.57
Fe_2O_3	1.88	2.51	1.80	1.70	1.38
MnO	0.01	0.04	0.02	0.01	0.04
MgO	0.30	0.38	0.34	0.36	0.29
CaO	1.15	1.31	0.62	1.33	1.21
Na_2O	2.95	2.75	2.71	3.04	3.26
K_2O	5.19	3.12	5.13	5.75	4.88
TiO_2	0.27	0.68	0.34	0.26	0.16
P_2O_5	0.73	0.28	0.08	0.08	0.09
LOI	0.63	0.54	0.53	–	–
Total	97.74	98.54	98.61	99.89	100.14
Rb	302.9	313.8	287.8	280.0	311.0
Cs	–	–	–	2.4	9.2
Pb	54.8	61.8	52.8	55.0	40.0
Ba	755.8	658.5	1559.8	910.0	690.0
Th	50.9	99.1	58.6	63.0	25.0
U	6.0	8.5	3.6	4.5	3.0
Nb	20.5	42.6	18.5	20.0	12.0
La	86.0	153.3	113.5	111.0	39.5
Ce	160.7	301.1	207.0	213.0	71.5
Sr	100.5	90.5	176.9	186.0	103.0
Pr	15.6	29.9	20.1	22.0	7.4
Nd	58.9	114.2	73.8	75.0	23.0
Zr	208.1	291.4	270.3	190.0	105.0
Sm	10.7	20.4	12.4	10.8	3.5
Eu	1.2	1.4	1.7	1.5	0.8
Gd	8.1	15.6	8.7	9.0	3.5
Tb	0.3	1.0	1.5	0.6	–
Dy	5.0	10.1	4.5	3.5	2.3
Y	74.1	48.4	19.9	15.0	10.5
Ho	0.7	1.4	0.6	0.6	0.3
Er	1.7	3.7	1.4	1.7	1.2
Tm	0.2	1.5	–	–	–
Yb	1.6	3.5	1.3	0.9	1.0
Lu	0.2	0.5	0.2	0.1	0.1
Zn	47.8	58.3	62.0	50.0	50.0
Cu	2.6	9.3	11.4	–	–
Ni	8.0	3.9	4.3	–	–
Cr	12.9	9.2	13.8	–	–
Co	37.5	27.1	29.9	15.0	12.5
Ga	18.1	19.1	18.5	24.0	20.0
Ge	–	–	–	–	–
Hf	6.2	8.2	7.5	6.0	3.0
Sn	6.2	3.4	2.5	1.0	6.0
Ta	1.6	4.9	2.0	5.5	7.0
W	27.3	20.8	22.9	22.7	106.0

for Ba, Nb–Ta, Sr, Eu and Zr–Hf (Fig. 18b). These features mark granitoids emplaced at convergent plate margins or originating from partial melting of crustal rocks. However, the discrimination diagram plots indicate that these are not arc granitoids and therefore their geochemical signature is inherited from partial melting of crustal rocks. The absence of any structural evidence for orogenic activity at ca. 1.65–1.55 Ga in central Africa suggests that this crustal melting event is unrelated to an orogeny and linked to underplating of hot mantle-originating magmas in the crust at that time.

5.2. Group III pre-Irumide plutonic rocks (1.34–1.33 Ga)

Group III intrusive bodies are known only in the far northeastern part of the Irumide belt, and consist of a nepheline syenite and deformed biotite granite. The nepheline syenite of Mivula Hill covers ~1 × 4 km (Newton, 1959; Tembo, 1986) and is located in the Muyombe area (Fig. 4). It is a medium-grained, locally porphyritic, nepheline-rich intrusion, with sodalite veinlets. Minor aegirine syenite and a sheared biotite syenite coexist with the nepheline syenite. The Ntendele biotite granite of the Muyombe sheet (Fig. 4) consists of foliated biotite granite, with stretched K-feldspar phenocrysts. The pluton was linked to the ca. 1930 Ma Nyika Granite suite by Ring et al. (1997).

A Rb–Sr date of 1341 ± 16 Ma (Fig. 5, Table 1, nos. 52 and 55) for the Mivula Hill syenite (Tembo, 1986) is supported by a $^{207}Pb/^{206}Pb$ evaporation date of 1360 ± 1 Ma (Vrána et al., 2004, Fig. 5, Table 1, nos. 52–55). The Ntendele biotite granite yielded a $^{207}Pb/^{206}Pb$ evaporation date of 1329 ± 1 Ma (Fig. 5, Table 1, no. 51, Vrána et al, 2004). These two dates indicate a ~1345 ± 15 Ma igneous event confined to the northernmost Irumide belt.

Major element analyses are reported for the Mivula syenite by Tembo (1986) and are given in Table 3. These data show relatively low SiO_2 (average 53.46 wt.%) versus high alkali (Na_2O: 5.30–11.65%; K_2O: 7.12–9.40%) and Al_2O_3 (19.52–24.86%) contents. MgO and CaO are in the range 0.11–1.22% and 0.35–3.84% respectively. These rocks contain normative nepheline and leucite. Their ASI is close to or lower than 1 (Fig. 17b) and their K_2O/Na_2O ratio is between 0.61 and 1.60 (Fig. 17c). Note however that the K/Na ratio is always <1. There are no REE data available for these rocks. Tembo (1986) pointed out there are no features supporting syn-orogenic intrusion of the Mivula syenite and therefore he suggested that this intrusive complex was emplaced in an anorogenic setting.

5.3. Group IV syn- to late-kinematic Irumide granitoids (1.05–0.95 Ga)

Syn- to late-kinematic Irumide granitoids include the Bemba Batholith (Lafila Granite), the Kaunga Granite and the Chilubanama Granite complexes in the northeastern Irumide belt and have been described in detail by Daly (1986). They also include large volumes of porphyritic granites throughout the belt. Group IV granitoids are homogeneous, with sharp intrusive contacts, and contain abundant xenoliths of Paleoproterozoic granite gneisses and metasedimentary rocks belonging to the Manshya River/Kanona Groups. The porphyritic granites are coarse grained and commonly contain abundant aligned microcline megacrysts. Solid-state fabrics in Group IV granitoids are heterogeneously distributed throughout the Irumide belt. A weak foliation is particularly developed near the margins of intrusive bodies, and the phenocrysts are aligned parallel to the margins. In some cases, a highly

Table 4d
Representative major and trace element geochemistry of Group IV granitoids in the central Irumide belt

	KTB1	MUN	CHL2	CHL4	CHL5	CHT1	CHT2	CHT4	CHT6	FW1
SiO_2	76.85	75.11	72.41	76.22	69.83	71.11	67.62	77.89	73.00	70.50
Al_2O_3	13.56	13.22	12.47	13.59	14.30	12.40	15.52	13.12	12.69	15.41
Fe_2O_3	0.87	2.13	3.49	0.79	5.13	5.91	5.87	0.75	5.20	3.87
MnO	–	–	–	–	–	–	–	–	–	–
MgO	0.18	0.11	0.22	0.21	1.04	1.07	2.18	0.14	0.69	1.18
CaO	0.58	0.88	1.80	0.66	3.27	3.42	1.23	0.51	1.77	2.44
Na_2O	2.43	2.58	2.92	3.26	2.69	2.48	1.87	3.51	2.61	2.77
K_2O	4.46	5.11	4.71	4.36	3.36	3.47	3.38	4.31	3.64	4.00
TiO_2	0.12	0.23	0.41	0.11	1.32	1.37	0.65	0.07	0.84	0.67
P_2O_5	0.06	0.07	0.13	0.15	0.21	0.14	0.13	0.13	0.18	0.12
LOI	0.01	0.00	0.01	0.01	0.01	0.01	0.02	0.01	0.02	0.01
Total	99.11	99.44	98.58	99.35	101.15	101.38	98.46	100.43	100.63	100.97
Rb	336.1	211.8	246.3	255.3	185.6	130.8	138.5	300.6	205.2	252.2
Cs	10.9	2.9	1.4	5.3	7.3	2.5	3.2	10.3	3.9	5.5
Pb	31.5	35.0	48.4	40.7	27.6	31.7	23.7	42.1	33.4	48.1
Ba	253.2	447.9	1694.6	426.8	1391.7	1650.0	818.5	277.2	959.6	1194.8
Th	6.1	29.7	33.8	13.1	9.8	22.8	17.9	11.9	16.9	50.2
U	2.4	2.2	1.7	5.5	2.1	2.0	1.9	7.1	1.7	3.5
Nb	18.8	23.0	28.0	14.7	6.6	12.2	14.6	21.6	16.7	13.0
La	18.2	131.7	128.9	23.2	52.1	81.6	43.5	18.5	57.0	91.5
Ce	39.1	284.7	180.2	42.9	118.4	176.1	95.2	30.4	121.4	193.0
Sr	55.8	36.0	101.3	59.5	149.7	153.2	126.4	54.7	125.7	291.0
Pr	5.5	26.6	25.7	3.8	12.0	20.4	8.4	3.2	13.3	17.7
Nd	23.4	93.6	98.5	13.8	45.9	81.6	31.8	11.6	51.3	56.6
Zr	157.8	176.2	74.3	101.0	96.7	52.0	218.4	53.9	52.7	236.2
Sm	6.1	19.1	20.5	3.0	10.1	16.5	7.3	3.3	12.6	10.4
Eu	1.0	1.1	3.2	0.5	2.1	2.8	0.9	0.6	1.9	1.5
Gd	5.8	13.8	20.2	2.6	7.6	13.5	5.3	3.5	10.7	6.1
Tb	1.0	2.5	3.7	0.6	1.4	2.4	0.9	0.8	2.1	1.0
Dy	5.4	11.2	19.0	2.6	6.9	12.6	3.8	4.5	10.9	4.8
Y	40.3	58.4	116.4	17.7	33.8	61.3	24.0	36.9	61.4	28.1
Ho	1.0	1.8	3.3	0.5	1.0	1.9	0.6	1.0	1.9	0.7
Er	2.5	5.2	10.3	1.5	2.9	5.7	2.1	2.9	5.2	2.2
Tm	0.4	0.8	1.6	0.2	0.5	0.9	0.3	0.6	0.9	0.4
Yb	2.9	5.1	10.1	1.4	3.0	5.0	2.1	3.4	6.1	2.4
Lu	0.4	0.8	1.6	0.3	0.5	0.9	0.4	0.6	0.9	0.3
Zn	24.8	79.7	96.9	24.7	115.9	117.7	106.8	24.5	85.3	70.1
Cu	15.5	2.3	5.6	2.7	15.2	7.5	15.2	3.1	23.0	18.1
Ni	3.1	2.8	4.1	2.9	6.7	3.8	56.8	2.9	6.4	11.6
Cr	9.0	8.7	9.0	9.4	14.4	8.5	137.9	8.5	16.0	27.2
Co	67.2	49.7	71.8	59.2	53.8	18.1	29.4	56.2	55.7	36.3
Ga	12.4	20.7	21.1	15.0	22.0	19.7	21.2	20.9	20.5	22.2
Ge	0.6	20.7	21.1	15.0	22.0	19.7	21.2	20.9	20.5	22.2
Hf	2.6	5.0	3.1	2.7	2.5	1.8	5.3	2.1	1.8	5.9
Sn	3.0	2.1	5.4	1.4	1.3	1.0	0.5	1.3	2.7	4.6
Ta	3.0	2.8	3.6	2.9	0.6	0.5	0.6	4.3	2.1	0.9
W	40.6	39.2	50.8	44.9	18.7	6.0	7.2	39.8	34.6	11.8

strained matrix wraps around rigid microcline phenocrysts in granitoids, while locally a mylonitic fabric occurs along northeast-trending shear zones.

Extensive shearing and mylonitisation has obscured the original contact between the Group II Mutangoshi Gneissic Granite and the younger Group IV Chilubanama Granite. However, subtle decrease of grain size in the Chilubanama Granite towards contact with the Mutangoshi Gneissic Granite, interpreted to record chilling of the former against the latter, and the presence of migmatitic granite pods within the Chilubanama Granite, interpreted as rafts of the Mutangoshi Gneissic Granite, suggest that the Mutangoshi Gneissic Granite and the unfoliated Chilubanama Granite are two distinct magmatic bodies. Two samples of what was previously mapped as the Mutangoshi Gneissic Granite near Chinsali (samples MTGG 1 and MTGG 2) yielded SHRIMP U–Pb zircon dates of 1027 ± 13 and 1055 ± 13 Ma (Fig. 9, Table 1, nos. 20 and 39). These samples were collected near the tectonised contact between the Mutangoshi Gneissic Granite and the Chilubanama Granite, and date the igneous crystallisation of the latter. Samples from strongly foliated and

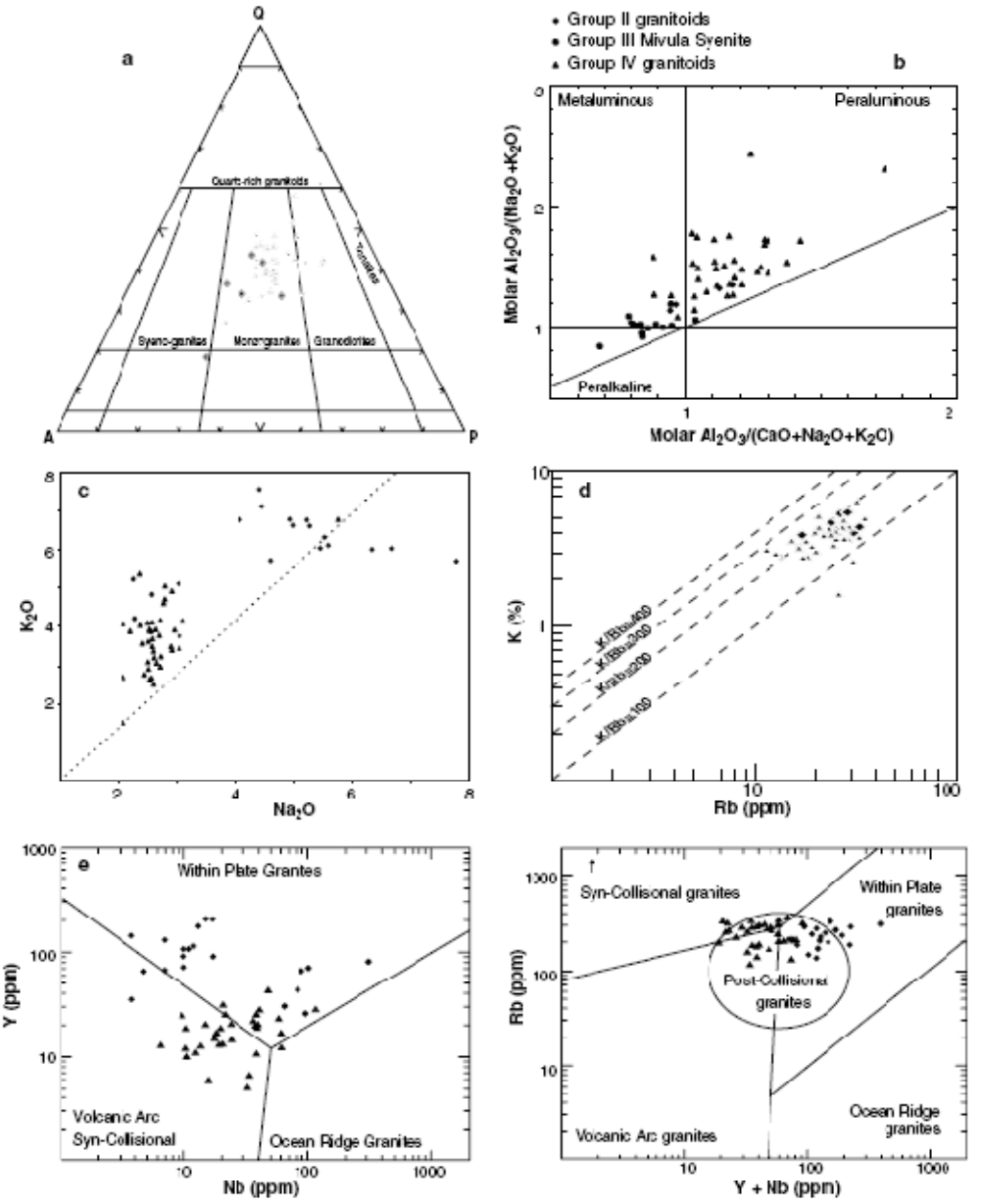

Fig. 17. (a) Q–A–P plot of Irumide granitoids (after Le Maitre 1989); (b) plot of $Al_2O_3/(Na_2O+K_2O)$ versus $Al_2O_3/(Na_2O+K_2O+CaO)$ (molar proportions) for Irumide granitoids afer Maniar and Piccoli (1989); (c) plot of K_2O versus Na_2O for Irumide granitoids; (d) Plot of Rb (ppm) versus K (%) after Shaw (1968) showing magmatic trends of Irumide granitoids; (e) position of Irumide belt granitoids in tectonic setting discrimination diagram after Pearce et al. (1984); (f) position of Irumide belt granitoids in tectonic setting discrimination diagram after Pearce (1996).

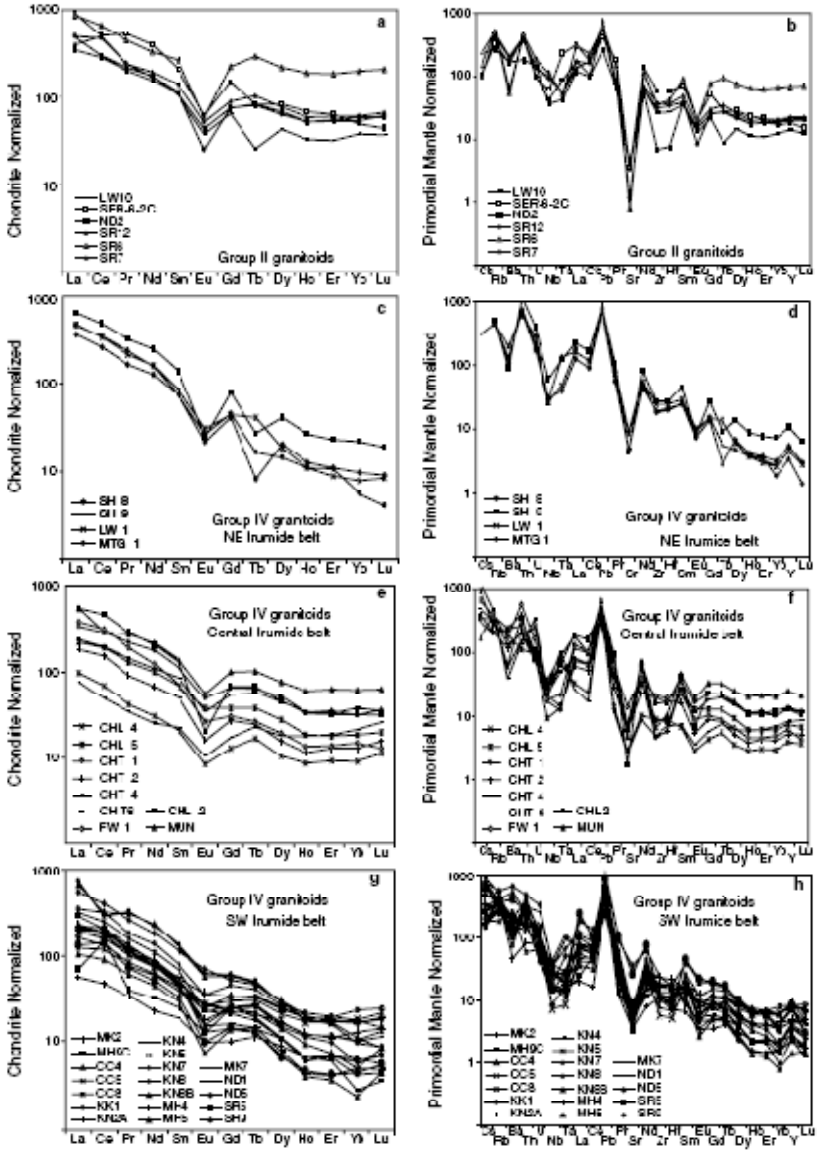

Fig. 18. (a) Chondrite-normalised REE plot for Irumide belt Group II granitoids. Normalisation values after McDonough and Sun (1995). (b) Primordial-mantle-normalised spider diagram for Irumide belt Group II granitoids. Normalisation values after Sun and McDonough (1989). (c,e,g) Chondrite-normalised REE plot for Irumide belt Group IV granitoids. Normalisation values after McDonough and Sun (1995). Diagrams (c), (e) and (g) are northeastern, central and southwestern Irumide belt respectively. (d,f,h) Primordial-mantle-normalised spider diagram for Irumide belt Group IV granitoids. Normalisation values after Sun and McDonough (1989). Diagrams (d), (f) and (h) are northeastern, central and southwestern Irumide belt respectively.

mylonitic Mutangoshi Gneissic Granite yielded a Rb–Sr whole-rock date of 1407 ± 33 Ma (Fig. 5, Table 1, no. 56, Daly, 1986). Apart from the two samples collected near the tectonised contact between the Chilubanama Granite and the Mutangoshi Gneissic Granite, no samples were collected from what can unequivocally be ascribed to the Mutangoshi Gneissic Granite. At this stage, the reported Rb–Sr age of Daly (1986) has not been confirmed by a U–Pb zircon date, but in our view could have been calculated using data that possibly includes phases of the Chilubanama Granite, and thus reflects a mixed age between Group II and Group IV granitoids. An alternative interpretation is that the age reflects partial resetting of the Rb–Sr system and can as such not be ascribed to a geological event.

Daly (1986) reported a nine-point Rb–Sr isochron of 947 ± 89 Ma for the Lufila Granite and a U–Pb zircon upper intercept age of 970 ± 5 Ma for the Kaunga Granite (Fig. 9, Table 1, nos. 3 and 4). SHRIMP U–Pb zircon dating by De Waele et al. (2002, 2003a,c) yielded crystallisation ages for Group IV granitoids ranging from 1.05 to 0.94 Ga as summarised in Table 1 and in Figs. 6–10. Near the junction between the Irumide and Ubendian belts, Ring et al. (1999) reported $^{207}Pb/^{206}Pb$ evaporation and TIMS zircon dates between 1.12 and 0.98 Ga (Fig. 5, Table 1, nos. 41, 43–47), but indicate that the dated granitoids occur within major shear zones, reactivated during the Mesoproterozoic and then during late Pan-African, at ca. 550 Ma (Ring, 1993; Ring et al., 1999).

Major element chemical characteristics of Group IV intrusive bodies (Tables 4a–4d) indicate a substantial compositional variation (SiO_2 = 64.65–77.89%, TiO_2 = 0.07–1.37%, Al_2O_3 = 12.14–16.17%, Fe_2O_3 = 0.69–5.91%, MgO = 0.11–2.48%, Na_2O = 1.86–3.63% and K_2O = 1.89–7.59%). In the normative classification diagram, the granitoids plot in the fields for monzogranite and granodiorite (Fig. 17a). They are metaluminous to peraluminous (Fig. 17b), with peraluminous compositions predominating (ASI = 0.88–1.73) and have K_2O/Na_2O ratios greater than 1 (Fig. 17c). The K/Rb ratios range from 110 to 266 and the data define a magmatic trend consistent with unaltered granitoids (Fig. 17d). The trace element concentrations are variable in Group IV granitoids (see Tables 4a–4d). In the discrimination diagrams of Pearce et al. (1984) and Pearce (1996), these granitoids plot in the fields for continental-collision-related syn- to post-orogenic granitoids, arc granites and within-plate granites (Fig. 17e and f). The dominance of peraluminous compositions and the emplacement during the paroxysm of D_2/M_2 or during the late- to post-kinematic stage of the Irumide orogeny indicate that these are not arc or anorogenic granitoids. They represent felsic melts originating from partial melting of the crust during the Irumide orogeny. The overlap between the age of these granitoids and the Barrovian-type metamorphism support this interpretation.

The REE abundances are 101–849 times chondrite (Fig. 18c, e and g). The REE patterns display a negative Eu anomaly ($Eu/Eu^* = 0.15–0.88$) and are characterised by La_N/Yb_N values in the range 9–74. The LREE display a fractionated pattern ($La_N/Sm_N = 2.8–6.6$), while the HREE are marked by sub-flat patterns with Gd_N/Yb_N between 1.5 and 9.0. The primordial-mantle-normalised patterns of these granitoids show negative anomalies for Ba, Nb–Ta, Ce, Sr, Eu and Zr–Hf (Fig. 18d, f and h). The geochemical data above are consistent with derivation from crustal partial melting in a convergent setting.

6. Regional implications and tectonic models

6.1. Age of pre-Irumide basement

The dominant pre-Irumide units exposed in the Irumide belt are ~2.05–1.85 Ga igneous rocks and closely related ~1.85 Ga Muva Supergroup metasedimentary rocks. These units represent the main component of the Bangweulu block, while Neoarchaean rocks represent a smaller component and are exposed at two localities in southeastern Zambia. The Archaean to Palaeoproterozoic Bangweulu block crust has been intruded by a suite of crust-originating granitoids between 1.65 and 1.55 Ga. Available data do not indicate a metamorphic event associated with the intrusion of these granitoids, and more work is needed to elucidate their significance in the tectonic evolution of central Africa.

6.2. Age of the Muva Supergroup

Previous workers (Daly and Unrug, 1982; Unrug, 1984) assumed that the Muva Supergroup is Mesoproterozoic in age. SHRIMP U–Pb zircon geochronological data reviewed in this paper (Table 1, Figs. 5 and 13) show instead that the Muva Supergroup was deposited between ca. 1.85 and 1.65 Ga. This is indicated by: (1) the absence of detrital zircon younger than ~1.85 Ga (Rainaud et al., 2003; De Waele and Fitzsimons, submitted for publication) and (2) ~1.88–1.85 Ga rhyolites interstratified within the Muva succession (De Waele and Fitzsimons, submitted for publication). These data indicate that deposition of the Muva Supergroup overlaps with emplacement of late-Ubendian potassic calc-alkaline volcanic and plutonic rocks in the Bangweulu block. Furthermore, the geochronological data support the coeval deposition of Manshya River Group quartzites and Mporokoso Group sedimentary rocks. As such, the Manshya River, Kanona and Mporokoso Group are related to the evolution of the Bangweulu block, and the adjacent Palaeoproterozoic Ubendian orogenic system, as previously suggested by Andersen and Unrug (1984), Kabengele et al. (1991) and Kapenda et al. (1998).

Tembo and Porada (submitted for publication) reviewed the distribution of the Muva quartzites and possible correlatives in Zambia and showed that they possibly extend outside the Irumide belt, e.g. within the Zambezi belt. They also suggested that these quartzites might be lateral corre-

latives of the abundant quartzites described in the Kibaran belt in Katanga, DRC. Hanson (2003) suggested, on this ground, that the southeast Kibaran (Katanga, DRC) and Muva (Zambia) sedimentary basins were originally continuous. Detrital provenance study on quartzites from the Kibaride belt in Katanga record 1.38 Ga detrital zircons (Kokonyangi et al., in press) and the same apply for part of the succession in the northern Kibaran belt (Cutten et al., 2004), placing a maximum age on these successions. The only sedimentary package within the Irumide belt that could possibly relate to these Mesoproterozoic sequences in central Africa is the Kasama Formation on the Bangweulu block, which contains detrital zircons as young as 1.43 Ga (De Waele and Fitzsimons, submitted for publication).

6.3. Timing of Irumide tectonism

Peak Irumide conditions have been constrained at 1021 ± 16 and 1004 ± 16 Ma through low Th/U zircon overgrowths in high-grade granitoids and gneisses within the Irumide belt s.s. (De Waele et al., 2003c, De Waele, 2005). Previous estimates in the southeastern parts of the Irumide belt place the timing of peak metamorphic conditions at 1046 ± 3 (Schenk and Appel, 2002) Ma and 1043 ± 19 Ma (Cox et al., 2002). These dates indicate a diachronous metamorphic front across strike, consistent with compressional arc tectonics along a convergent margin.

6.4. Irumide basin

The first modern tectonic interpretation of the Irumide belt is that of Daly (1986) who proposed that the belt formed during closure of a Mesoproterozoic marine basin within which the Muva Supergroup had accumulated. However, the data in this paper show that there is no evidence for an extensional sedimentary basin (equivalent to the first-stage of the Wilson-cycle) that opened after the Palaeoproterozoic Ubendian orogeny and was filled by sedimentary sequences that underwent orogenesis for the first time during the late Mesoproterozoic Irumide orogeny. In fact, the Manshya River/Kanona Group succession of the Irumide belt represents the deformed Ubendian molasse sequence, while the Mporokoso Group on the Bangweulu block foreland to the Irumide belt represents the undeformed Ubendian molasses. To date, extensive Mesoproterozoic successions deposited along the southern margin of the Bangweulu block are yet to be identified. In our view, the exposed part of the Irumide belt lies outside the main site of closure of a Mesoproterozoic ocean to the southeast. Mesoproterozoic oceanic crust has been documented to the southeast of the Irumide belt in the 1.4 Ga Chewore complex in Zimbabwe (Johnson, 1999), providing evidence of an oceanic realm to the southeast as far back as 1.4 Ga. A series of juvenile magmatic arcs have been recognised in southern Malawi (1.04–1.00 Ga, Kröner et al., 1999), northwestern Mozambique (1.05–1.01 Ga, Kröner et al., 1997, 2000; Manhica et al., 2001), northern Zimbabwe (1.10–1.05 Ga, Johnson and Oliver, 2004) and central Zambia (~1.10 Ga, Hanson, 1999; Katongo et al., 2004) and are interpreted to have been accreted to the southern margin of the Bangweulu block during Irumide tectonism.

6.5. "Pop-up" model

The double vergence "pop-up" model proposed by Daly (1986) in the southwestern Irumide, was based on the recognition of upright structures and amphibolite facies rocks marking the core of a doubly-vergent tectonic complex. However, lithologies assigned by Daly (1986) to a Palaeoproterozoic culmination in that pop-up structure have been shown to be late Irumide in age. De Waele and Mapani (2002) considered the southeast-verging thrusts to represent back-thrusts within the main northwest-directed thick-skinned Irumide thrusts, possibly formed in response to basement topography. Although the presence of abundant Irumide-age granitoids rather than Palaeoproterozoic basement does not invalidate the "pop-up" model, the tectonic significance of the structure is greatly reduced.

6.6. Tectonic models

6.6.1. Geochemical indicators

The peraluminous Group IV Irumide granitoids display relatively high SiO_2 contents, with Aluminium Saturation Index values indicating a predominance of strongly peraluminous compositions. The geochemical characteristics of these granitoids could suggest the involvement of a broad spectrum of source lithologies during their genesis, i.e. they could have originated from partial melting of metamorphosed igneous and sedimentary rocks. The large volume of ca. 1.05–1.02 Ga granitoids within the Irumide belt, all displaying similar geochemical traits marked by enrichment in LILE and depletion in HFS elements is consistent with their generation from extensive crustal melting. Magmatic underplating is commonly described as an important process of crustal growth in a wide variety of setting, including accretionary and collisional orogens (Moores and Twiss, 1995) and could have provided the heat-source required for large-scale crustal anatexis. The structural data show that the peraluminous Group IV granitoids are syn-to late-kinematic compared to the climax of the Irumide orogeny, and SHRIMP U–Pb geochronological data (Table 1) indicate that they are broadly coeval with a metamorphic event dated at ~1021–1012 Ma. The geochemical evidence to date supports the notion that the Irumide belt s.s. represents the intensely reworked margin of the Palaeoproterozoic Bangweulu block.

6.6.2. Metamorphic indicators

The regional metamorphic grade in the Irumide belt is of medium pressure/medium temperature Barrovian type, which is more consistent with an accretionary setting then a continent–continent collision. Although no quantitative

data are available, preliminary *P–T–t* models suggest a clockwise metamorphic *P–T–t* path (Mapani, 1999) that is here linked to the major shortening event recorded by northwest-vergent thrusts. A younger anti-clockwise *P–T–t* path recognised locally in the Irumide belt could mark post-orogenic crustal extension but there is no structural evidence to support this interpretation. In our interpretation, the central high-grade part of the belt, previously inferred to represent a "pop-up" structure (Daly, 1986) represents a major zone of syn- to late-kinematic plutonism, creating a high thermal gradient in the crust causing an anti-clockwise *P–T–t* path. More geochemical and possibly isotopic data are required in order to more reliably constrain the origin of the Irumide igneous rocks. Peak metamorphic constraints for the Irumide belt are 30 M.y. younger than those recorded in the southeastern extent of the belt. This diachroneity is thought to reflect compressional continental-margin arc tectonics, in which continental and/or oceanic arcs are accreted to the southern margin of the Bangweulu block during Irumide tectonism.

6.7. Regional correlations

Shackleton (1973) and Hanson et al. (1988) suggested that the Irumide belt and the Choma–Kalomo block were two segments of the same belt cross-cut by the Neoproterozoic Zambezi belt. Kampunzu et al. (1991, 1993, 2000) showed that igneous rocks exposed in the adjacent Damaran-Katangan segments of the Pan African orogenic system represent continental rift and Red-Sea-type mafic rocks, supporting limited development of Neoproterozoic seafloor along this trend, and therefore allowing the possibility of a linkage between the Irumide belt and Choma–Kalomo block. However, based on the presence of yoderite-bearing whiteschists in the Zambezi belt, Johnson and Oliver (2000) argue for the closure of a major Neoproterozoic ocean during convergence between the Congo and Kalahari cratons. John et al. (2003, 2004) consider the eclogites within the Zambezi belt and the Lufilian Arc to represent relict oceanic crust. The eclogites record low geothermal gradients during metamorphism (~8 °C/km) and have been subducted to depths of ~90 km. John et al. (2001, 2003, 2004) take this to indicate the presence of a mature ocean basin that separated the Congo and Kalahari cratons prior to Pan African orogenesis. This interpretation would make it unlikely that the Choma–Kalomo block would be the southwestern extension of the Irumide belt. Geological and geochronological data presented in this paper show that the timing of magmatic events in the Irumide belt differs substantially from that in the Choma–Kalomo block. The critical differences between these two terranes are the following: (a) Palaeoproterozoic rocks are widespread and form the bulk of the crustal section affected by late Mesoproterozoic shortening in the Irumide belt. In contrast, Palaeoproterozoic rocks are unknown in the Choma–Kalomo block (Hanson et al., 1988); (b) granitoids emplaced between 1.4 and 1.2 Ga form large parts of the Choma–Kalomo block (Hanson et al., 1988) and their geochemical features suggest that they represent peraluminous felsic melts possibly originating from crustal anatexis (Bulambo et al., 2004). In contrast, peraluminous granitoids in that age range are unknown in the Irumide belt (De Waele et al., 2003c). A minor nepheline–sodalite syenite and a biotite granite gneiss dated by Tembo (1986) and Vrána et al. (2004) and a suite of A-type granitoids in northern Zambia outside the main Irumide belt (Ring et al., 1999) are time-correlatives of granitoids exposed in the Choma–Kalomo block and in the Kibaride belt. Their petrological characteristics however suggest emplacement in an anorogenic setting and thus unrelated to the evolution of the younger (~1.05–0.95 Ga) Irumide belt. Although these data are not consistent with a direct linkage between the Choma–Kalomo block and the Irumide belt, and lend support to the interpretation of Johnson and Oliver (2000), John (2001) and John et al. (2003, 2004), they do not provide direct proof for the development of a large Neoproterozoic ocean basin between the Congo and Kalahari cratons. Elucidating the complex Neoproterozoic evolution of this part of Africa requires further research.

Acknowledgements

This work has been made possible through the financial and logistical support from the Geology Department at the University of Zambia, the Australian Research Council (ARC) through the Tectonic Special Research Centre, and a Curtin University International Postgraduate Research Scholarship (IPRS) awarded to B.D.W. We acknowledge the support of Watling, Pritchard and Fjastad for the geochemical analyses conducted at the School of Applied Chemistry, Curtin University. A.B.K. acknowledges the financial support of the University of Botswana (1995–2001), the University of Lubumbashi (1976–1995) and the IGCP 440 that allowed him to reach his current understanding of the Bangweulu block in DRC and Zambia. Lubala, Kapenda, Kabengele and Tshimanga are acknowledged for their collaboration with A.B.K. during the study of the Congolese section of the Bangweulu block. This paper is TSRC Publication 257 and is a contribution to the International Geological Correlation Projects 418 and 440.

References

Ackermann, E.H., 1936. Das problem der Mkushi-Gneise am NW-rand der Rhodesischen masse. Geologische Rundschau 27, 81–87.

Ackermann, E.H., 1950. Ein neuer faltengurtel in Nordrhodesien und seine tectonische stellung im Afrikanishen grundgebirge. Geologische Rundschau 38, 24–39.

Ackermann, E.H., 1960. Strukturen im untergrund eines intrakratonischen doppelorogens (Irumiden Nordrhodesien). Geologische Rundschau 50, 538–553.

Ackermann, E.H., Forster, A., 1960. Grundzuge der stratigraphie und struktur des Irumide Orogen. In: 21st International Geological Congress, pp. 182–192.

Agar, R.A., Ray, A.K., 1983. The geological map of the Petauke area (1:250 000). Geological Survey of Zambia, Lusaka.

Andersen L.S., Unrug, R., 1984. Geodynamic evolution of the Bangweulu block, northern Zambia. Precambrian Research 25, 187–212.

Andrews-Speed, C.P., 1986. Gold-bearing fluvial and associated tidal marine sediments of Proterozoic age in the Mporokoso basin, northern Zambia. Sedimentary Geology 48, 193–222.

Andrews-Speed, C.P., 1989. The Mid-Proterozoic Mporokoso basin, northern Zambia: sequence stratigraphy, tectonic setting and potential for gold and uranium mineralisation. Precambrian Research 44, 1–17.

Andrews-Speed, C.P., Unrug, R., 1982. Gold in the sedimentary cover of the Bangweulu block, northern Zambia. Gold 82, 221–237.

Ayres, H.R., 1974. The geology of the Shiwa N'Gandu area; explanation of degree sheet 1131, NE quarter. Report Geological Survey Zambia 64.

Barr, M.W.C., Dryslall, A.R., 1972. The geology of the Sasare area; explanation of degree sheet 1131, SW quarter. Report Geological Survey of Zambia 30.

Brewer, M.S., Haslam, H.W., Darbyshire, P.F.P., Davis, A.E., 1979. Rb–Sr age determinations in the Bangweulu block, Luapula Province, Zambia, Institute of Geological Sciences London 79-5, 11p.

Bulambo, M., De Waele, B., Kampunzu, A.B., Tembo, F., 2004. SHRIMP U–Pb geochronology of the Choma–Kalomo block (Zambia) and geological implications. In: 20th Colloquium of African Geology, Orléans, France.

Carruthers, H., 2003. The geological map of the Chin'gombe area. Geological Survey Department of Zambia, Lusaka.

Chisela, S., 2000. The geological map of the Kakula area. Geological Survey Department of Zambia, Lusaka.

Cordiner, R.J., 1977. The geology of the Chitambo mission area; explanation of degree sheet 1230, SE quarter. Report Geological Survey Department of Zambia 54.

Cordiner, R.J., 2000. The geological map of the Kanona area. The Geological Survey Department of Zambia, Lusaka.

Cox, R.A., Rivers, T., Mapani, B., Tembo, D., De Waele, B., 2002. New U–Pb data for the Irumide belt: LAM–ICP–MS results for Luangwa Terrane. In: Geological Society of Namibia (Ed.), 11th IAGOD Quadrennial Symposium and Geocongress, Windhoek, Namibia, 3p.

Cutten, H., De Waele, B., Ferrandez-Alonso, M., Tack, L., 2004. Age constraints for basin evolution and sedimentation in the "Northeastern Kibaran Belt". In: 20th Colloquium of African Geology, Orléans, France.

Cvetcovic, D., 1973. The geology of the Mita hills area; explanation of degree sheet 1429, NW quarter. Report Geological Survey Department of Zambia 34.

Daly, M.C., 1986. The Tectonic and Thermal Evolution of the Irumide Belt, Zambia. PhD Thesis, University of Leeds, 326p.

Daly, M.C., 1994a. The geological map of the Chinsali area (1:100,000). Geological Survey Department of Zambia, Lusaka.

Daly, M.C., 1994b. The geological map of the Isoka area (1:100,000). Geological Survey Department of Zambia, Lusaka.

Daly, M.C., 1994c. The geological map of the Mulilansolo Mission area (1:100 000). Geological Survey Department of Zambia, Lusaka.

Daly, M.C., 1995. The geology of Mulilansolo Mission and Isoka areas; explanation of degree sheet 1032, NE and NW quarter. Report Geological Survey Department of Zambia 84.

Daly, M.C., Unrug, R., 1982. The Muva Supergroup, northern Zambia. Transactions of the Geological Society of South Africa 85, 155–165.

De Waele, B., 2005. The Proterozoic geological history of the Irumide belt. Zambia. PhD Thesis, Curtin University of Technology, Perth, 468 pp.

De Waele, B., Fitzsimons, I.C.W., submitted for publication. The nature and timing of Palaeoproterozoic sedimentation around the Bangweulu block of northern Zambia. Journal of the Geological Society of London.

De Waele, B., Mapani, B., 2002. Geology and correlation of the central Irumide belt. Journal of African Earth Sciences 35 (3), 385–397.

De Waele, B., Wingate, M.T.D., Mapani, B., 2002. Geochronological constraints on granitoid magmatism and deformation in the southwestern Irumide belt, Zambia. In: Geological Survey of Namibia (Ed.), 11th IAGOD Quadrennial Symposium and Geocongress, Windhoek, Namibia, p. 3.

De Waele, B., Fitzsimons, I.C.W., Wingate, M.T.D., Mapani, B., 2003a. The tectonothermal history of the Irumide belt of Zambia. Regional significance of new geochronological constraints. In: Li, H., Zhang, S. (Eds.), Assembly and Breakup of Rodinia, South China Field Symposium, Chengdu Institute of Geology and Mineral Resources, China Geological Survey, Hangzhou, China, pp. 16–19.

De Waele, B., Nemchin, A.A., Kampunzu, A.B., 2003b. The Bangweulu block of northern Zambia: where is the pre-Ubendian crust? In: Li, H., Zhang, S. (Eds.), Assembly and Breakup of Rodinia, South China Field Symposium, Chengdu Institute of Geology and Mineral Resources, China Geological Survey, Hangzhou, China, pp. 19–21.

De Waele, B., Wingate, M.T.D., Mapani, B., Fitzsimons, I.C.W., 2003c. Untying the Kibaran knot: a reassessment of Mesoproterozoic correlations in southern Africa based on SHRIMP U–Pb data from the Irumide belt. Geology 31 (6), 509–512.

De Waele, B., Liégeois, J.P., Nemchin, A.A., Tembo, F., 2005. Isotopic and geochemical evidence of Proterozoic episodic crustal reworking within the Irumide Belt of south-central Africa, the southern metacratonic boundary of an Archaean Bangweulu Craton. Precambrian Research.

Dodson, M.H., Cavanagh, B.J., Thatcher, E.C., Aftalion, M., 1975. Age limits for the Ubendian metamorphic episode in northern Malawi. Geological Magazine 112, 403–410.

Drysdall, A.R., Johnson, R.L., Moore, T.A., Thieme, J.G., 1972. Outline of the geology of Zambia. Geologie en Mijnbouw 51, 265–276.

Fitches, W.R., 1968. Structural and Stratigraphic Relations in the Precambrian Rocks of the Mafingi Hills Area of Northern Malawi and Zambia. PhD Thesis, University of Leeds.

Fitches, W.R., 1971. Sedimentation and tectonics at the northern end of the Irumide orogenic belt, northern Malawi and Zambia. Geologische Rundschau 59, 444–458.

Forster, A., 1965. Der kristallin sockel im ostlichen Nordrhodesien und sein verband mit anderen baueinheiten zentral- und Ostafrikas. Geotektonische Forschungen 20 (I–II), 115.

Hanson, R.E., 1999. The Mpande Gneiss. In: De Waele, B., Tembo, F., Key, R.M. (Eds.), Fieldtrip Guide: The Zambian Irumide belt. Geological Society of Zambia, Lusaka.

Hanson, R.E., 2003. Proterozoic geochronology and tectonic evolution of southern Africa. In: Yoshida M., Windley, B.F., Dasgupta, S.(Eds.), Proterozoic East Gondwana: Supercontinent Assembly and Breakup. Geological Society of London, pp. 427–463.

Hanson, R.E., Wilson, T.J., Brueckner, H.K., Onstott, T.C., Wardlaw, M.S., Johns, C.C., Hardcastle, K.C., 1988. Reconnaissance geochronology, tectonothermal evolution, and regional significance of the middle Proterozoic Choma-Kalomo block, southern Zambia. Precambrian Research 42, 39–61.

Haslam, H.W., Rundle, C.C., Brewer, M.S., 1986. Rb–Sr studies of metamorphic and igneous events in eastern Zambia. Journal of African Earth Sciences 5 (5), 447–453.

John, T., 2001. Subduction and Continental Collision in the Lufilian Arc–Zambezi Belt Orogen: A Petrological, Geochemical, and Geochronological Study of Eclogites and Whiteschists (Zambia). PhD Thesis, Kiel, 78 p.

John, T., Schenk, V., Haase, K., Scherer, E., Tembo, F., 2003. Evidence for a Neoproterozoic ocean in south-central Africa from mid-oceanic-ridge-type geochemical signatures and pressure-temperature estimates of Zambian eclogites. Geology 31 (3), 243–246.

John, T., Schenk, V., Mezger, K., Tembo, F., 2004. Timing and PT evolution of whiteschist metamorphism in the Lufilian arc–Zambezi belt Orogen (Zambia): implications for the assembly of Gondwana. Journal of Geology 112, 71–90.

Johns, C.C., Liyungu, K., Mabidi, S., Msale, G., Salungo, F., Tembo, D., Vallance, G., Barr, M.W.C., 1989. The stratigraphic and structural framework of eastern Zambia: results of a geotraverse. Journal of African Earth Sciences 9, 123–136.

Johnson, S., 1999. A Kibaran-aged marginal basin and island-arc complex in northern Zimbabwe. In: De Waele, B., Tembo, F., Key, R.M.

(Eds.), Abstracts Volume IGCP 418/419. Geological Society of Zambia. Lusaka, p. 6.

Johnson, S.P., Oliver, G.J.H., 2000. Mesoproterozoic oceanic subduction, island-arc formation and the initiation of back-arc spreading in the Kibaran belt of central, southern Africa: evidence from the ophiolite terrane, Chewore Inliers, northern Zimbabwe. Precambrian Research 103, 125–146.

Johnson, S.P., Oliver, G.J.H., 2004. Tectonothermal history of the Karousa arc, northern Zimbabwe. Precambrian Research 130, 71–97.

Johnson, S.P., Rivers, T., De Waele, B., 2005. A review of the Mesoproterozoic to early Palaeozoic magmatic and tectonothermal history of south-central Africa: implications for Rodinia and Gondwana. Journal of the Geological Society of London 162, 433–450.

Kabengele, M., Lubala, R.T., Cahen, B., 1991. Caractérisation pétrologiques et géochimique du magmatisme ubendien du secteur de Pepa-Lubumba, sur le plateau des Marungu (Nord-Est du Shaba, Zaire). Signification géodynamique dans l'évolution de la chaine ubeadienne. Journal of African Earth Sciences 13 (2), 243–265.

Kampunzu, A.B., Kapenda, D., Manteka, B., 1991. Basic magmatism and geotectonic evolution of the Par African belt in central Africa: evidence from the Katangan and west Congolian segments. Tectonophysics 190, 363–371.

Kampunzu, A.B., Kanika, M., Kapenda, D., Tshimanga, K., 1993. Geochemistry and geotectonic setting of late Proterozoic Katangan basic rocks from Kibambale in Central Shaba (Zaire). Geologische Rundschau 82, 619–630.

Kampunzu, A.B., Tembo, F., Matheis, G., Kapenda, D., Huntsman-Mapila, P., 2000. Geochemistry and tectonic setting of mafic igneous units in the Neoproterozoic Katangan Basin, central Africa; implications for Rodinia break-up. Gondwana Research 3, 125–153.

Kapenda, D., Kampunzu, A.B., Canalis, B., Namegabe, M., Tshimanga, K., 1998. Petrology and geochemistry of post-kinematic mafic rocks from the Palaeoproterozoic Ubeadian belt, NE Katanga (DRC). Geologische Rundschau 87, 345–362.

Katongo, C., Köller, F., Klötzli, U., Koeberl, C., Tembo, F., De Waele, B., 2004. Petrography, geochemistry and geochronology of key granitoid rocks in the Neoproterozoic–Palaeozoic Lufilian–Zambezi belt, Zambia: implications for the tectonic setting and regional correlation. Journal of African Earth Sciences 40 (5), 219–244.

Kerr, C.D., 1975. The geology of the Piwila mission area; explanation of degree sheet 1325, SE quarter. Report Geological Survey Department of Zambia 68.

Key, R.M., Liyungu, A.K., Njamu, F.M., Somwe, V., Banda, J., Mosley, P.N., Armstrong, R.A., 2001. The western arm of the Lufilian arc in NW Zambia and its potential for copper mineralisation. Journal of African Earth Sciences 33, 503–528.

Kinnaird, J.A., Bowden, P., 1991. Magmatism and mineralisation associated with Phanerozoic anorogenic plutonic complexes of the African Plate. In: Kampunzu, A.B., Lubala, R.T. (Eds.), Magmatism in Extensional Structural Settings: The Phanerozoic African Plate. Springer-Verlag, Berlin, pp. 410–485.

Klerkx, J., Theunissen, K., Delvaux, D., 1998. Persistent fault controlled basin formation since the Proterozoic along the western branch of the East African Rift. Journal of African Earth Sciences 26, 347–361.

Kokonyangi, J., Kampunzu, A.B., Armstrong, R., Ngulube, D.A., Yoshida, M., Okudaira, T., in press. The Mesoproterozoic Kibaride belt (Katanga, SE D.R. Congo). Journal of African Earth Sciences, doi:10.1016/j.jafrearsci.2006.01.017.

Kröner, A., Sacchi, R., Jaeckel, P., Costa, M., 1997. Kibaran magmatism and Par-African granulite metamorphism in northern Mozambique: single zircon ages and regional implications. Journal of African Earth Sciences 25 (3), 467–484.

Kröner, A., Windley, B.F., Jaeckel, P., Collins, A.S., Brewer, T.S., Nemchin, A., Razakamanana, T., 1999. New zircon ages for Precambrian granites, gneisses and granulites from central and southern Madagascar: significance for correlations in East Gondwana. Gondwana Research 2 (3), 351–352.

Kröner, A., Eirks, P.H.G.M., Jamal, D.L., 2000. Archaean, Kibaran and Pan-African zircon ages for granitoic rocks in northwestern Mozambique, Geo Luanda. Luanda, Angola.

Le Maître, R.W., 1988. A classification of igneous rocks and glossary of terms: recommendations of the International Union of Geological Sciences subcommission on the systematics of igneous rocks. Blackwell, Oxford, 193 pp..

Liyungu, K., Vinyu, M., 1996. Constrains on the timing of the high-grade Lutembwe quartz-feldspathic granulite, charnockitic enderbite and the relationship to the Chipata granite in the Mozambique belt. In: Kamona, F., Tembo, F., Mapani, B.S.E. (Eds.), IGCP 363: Palaeoproterozoic of sub-Equatorial Africa. Geological Society of Zambia, Lusaka, p. 19.

Lucazik, E., 1998. The geology of the Ilendola Mission area; explaration of degree sheet 1031, SE quarter. Report Geological Survey Department of Zambia 95.

Maniar, P.D., Piccoli, P.M., 1989. Tectonic discrimination of granitoids. Geological Society of America Bulletin 101, 635–643.

Manhica, A.D.S.T., Grantham, G.H., Armstrong, R.A., Guise, P.G., Kruger, F.J., 2001. Polyphase deformation and metamorphism at the Kalahari craton-Mozambique belt boundary. In: Miller, J.A., Holdsworth, R.A., Buick, I.S., Hand, M. (Eds.), Continental Reactivation and Reworking. Geological Society of London, pp. 303–322.

Mapani, B., 1999. Tectonic and metamorphic evolution of the Serenje and adjoining areas. In: De Waele, B., Tembo, F., Key, R.M. (Eds.), Abstracts Volume IGCP 418/419. Geological Society of Zambia, Lusaka, p. 16.

Mapani, B.S.E., Moore, T.A., 1995. The geology of the Serenje area; explanation of degree sheet 1330, NW quarter. Report Geological Survey Department of Zambia 51.

Mapani, B.S.E., Rivers, T., Tembo, F., Katongo, C., 2001. Terrane mapping in the eastern Irumide and Mozambique belts: implications for the assembly and dispersal of Rodinia. In: McCourt, S. (Ed.), IGCP 418 4th fieldmeeting. University of Durban-Westville, Durban, South Africa.

Marten, B.E., 1968. The geology of the Chalabesa Mission area; explanation of degree sheet 1131, NW quarter. Report Geological Survey Department of Zambia 23.

McDonough, W.F., Sun, S.-S., 1995. The composion of the Earth. Chemical Geology 120, 228.

Moore, T.A., 1967. The geology of the Ndola and Bwana Mkubwa areas; explanation of degee sheets 1228, part of SE quarter, and 1328, part of NE quarter. Report Geological Survey Department of Zambia 20.

Moores, E.M., Twiss, R.J., 1995. Tectonics. W.H. Freeman and Company, New York, 415p.

Mosley, P.N., 1979. The geology of the Mofwe area; explanation of degree sheet 1132, SW quarter. Report Geological Survey Department of Zambia 82.

Mosley, P.N., Marten, B.S., 1979. The geology of the Katibunga mission area; explanation of degree sheet 1131, SE quarter. Report Geological Survey Department of Zambia 81.

Namateba, C., 1994. The geology of the Mafinga Hills area; explaration of degree sheet 0933, SW quarter. Report Geological Survey Department of Zambia 93.

Newton, A.R., 1959. On the syerite of Mivula Hill, eastern province. Records of the Geological Survey of Zambia 1957, 14–17.

Ngoyi, K., Liégeois, J.-P., Demaiffe, D., Dumont, P., 1991. Age tardi-ubendien (Protérozoïque inférieur) des dômes granitiques de l'arc capriférè zaïro-zambien. Comptes Rendu de l'Academie de Sciences 313 (II), 83–89.

Page, T.C., 1973. The geology of the Chilonga Mission area; explaration of degree sheet 1231, NW quarter. Report Geological Survey Department of Zambia 56.

Pearce, J.A., 1996. Sources and settings of granitic rocks. Episodes 19, 120–125.

Pearce, JA., Harris, N.B.W., Tindle, A.G., 1984. Trace element discrimination diagrams for the tectonic interpretation of granitic rocks. Journal of Petrology 25, 956–983.

Phillips, K.A., 1960. The geology of the Sirda area; explanation of degree sheet 1431, NE quarter. Report Geological Survey of Zambia 9.

Phillips, K.A., 1964. The geology of the Lusandwa River area; explanation of degree sheet 1331, SE quarter. Report Geological Survey of Zambia 13.

Phillips, K.A., 1965. The geology of the Petauke – Mwanjawantu area; explanation of degree sheet 1431, NW and part of SW quarters. Report Geological Survey of Zambia 15.

Pitcher, W.S., 1997. The Nature and Origin of Granite. Chapman & Hall, London, 408p.

Rainaud, C., Master, S., Armstrong, R.A., Robb, L.J., 2003. A cryptic Mesoarchaean terrane in the basement to the central African Copperbelt. Journal of the Geological Society of London 160, 11–14.

Rainaud, C.L., Armstrong, R.A., Master, S., Robb, L.J., Mumba, P.A.C.C., 2002. Contributions to the geology and mineralisation of the central African Copperbelt: I. Nature and geochronology of the pre-Katangan basement. In: Geological Survey of Namibia (Ed.), 11th IAGOD Quadrennial Symposium and Geocongress, Windhoek, Namibia, p. 5.

Rainaud, C., Master, S., Armstrong, R.A., Robb, L.J., 2005. Geochronology and nature of the Palaeoproterozoic basement in the Central African Copperbelt (Zambia and the Democratic Republic of Congo), with regional implications. Journal of African Earth Sciences 42, 1–31.

Ramsay, C.R., Ridgway, J., 1977. Metamorphic patterns in Zambia and their bearing on problems of Zambuan tectonic history. Precambrian Research 4, 321–337.

Reichwalder, P., Brandon, A., 1992. The geological map of the Luano Valley area. Geological Survey Department of Zambia, Lusaka.

Ridgway, J., Ramsay, C.R., 1986. A provisional metamorphic map of Zambia – explanatory notes. Journal of African Earth Sciences 5 (5), 441–446.

Ring, U., 1993. Aspects of the kinematic history and mechanisms of superposition of the Proterozoic mobile belts of eastern central Africa (northern Malawi and southern Tanzania). Precambrian Research 62, 207–226.

Ring, U., Kröner, A., Toulkeredis, T., 1997. Palaeoproterozoic granulite-facies metamorphism and granitoid intrusions in the Ubendian–Usagaran Orogen of northern Malawi, east-central Africa. Precambrian Research 85, 27–51.

Ring, U., Kröner, A., Layer, P., Buchwaldt, R., Toulkeredis, T., 1999. Deformed A-type granites in northern Malawi, east-central Africa: pre- or syntectonic. Journal of the Geological Society of London 156, 695–714.

Schandelmeier, H., 1980. Regionale gliederung des Prakambriums und aspekte der krustentwicklung um Mambwe/nordost-Zambia. PhD Thesis, Technical University of Berlin, Berlin, 134 p.

Schandelmeier, H., 1981. The Precambrian of NE Zambia in relation to the dated Kate, Mambwe and Luchewe intrusives. Geologische Rundschau 70 (2), 956–971.

Schandelmeier, H., 1983. The geochronology of post-Ubendian granitoids and dolerites from the Mambwe area, northern Province, Zambia. Report Institute of Geological Sciences 83 (1), 40–46.

Schenk, V., Appel, P., 2001. Anti-clockwise P–T path during ultrahigh-temperature (UHT) metamorphism at ca. 1050 Ma in the Irumide belt of eastern Zambia. Berichte der Deutschen Mineralogischen Gesellschaft, Beihefte zum European Journal of Mineralogy 13, 161.

Schenk, V., Appel, P., 2002. UHT-metamorphism in the Irumide belt of Zambia: an anti-clockwise P–T path and concordant monazite age at 1.05 Ga. In: Ennih, N., Abdelsalam, M.G. (Eds.), 19th Colloquium of African Geology, El Jadida, Morocco, p. 165.

Shackleton, R.M., 1973. Correlation of structures across Precambrian orogenic belts in Africa. In: Tarling, D.H., Runcorn, S.K. (Eds.), Implications of Continental Drift to the Earth Sciences. Academic press, London, pp. 1091–1095.

Shaw, D.M., 1968. A review of K–Rb fractionation trends by covariance analysis. Geochimica et Cosmochimica Acta 32, 573–601.

Smith, A.G., 1966. The geology of the Kapri Mposhi area; explanation of degree sheet 1328, SE quarter. Report Geological Survey Department of Zambia 18.

Smith, A.G., Kerr, C.D., 1975. The geology of the Ndabala area; explanation of degree sheet 1329, NE quarter. Report Geological Survey Department of Zambia 67.

Steiger, R.H., Jäger, E., 1977. Subcommission on geochronology: convention on the use of decay constants in geo- and cosmochronology. Earth and Planetary Science Letters 36, 359–362.

Stillman, C.J., 1965. The geology of the Macofu river and Mkushi areas; explanation of degree sheet 1329, part of NW quarter, and SW quarter. Report Geological Survey Department of Zambia 12.

Sun, S., McDonough, W.F., 1989. Chemical and isotopic systematics of ocean basalts: implications for mantle composition and processes. In: Saunders, A.D.N., Norry, M.J. (Eds.), Magmatism in the Ocean Basins. Geological Society of London Special Publication, pp. 313–345.

Sykes, J.M.D., 1995. The geology of the Luswa River area, explanations of degree sheet 1132, NW quarter. Report Geological Survey Department 76.

Sylvester, P.I., 1989. Post-collisional alkaline granites. Journal of Geology 97, 261–280.

Tembo, F., 1986. Petrology and Geochemistry of Syenite Intrusions in the Eastern Province of Zambia. Msc. Thesis, University of Zambia, Lusaka.

Tembo, F., Porada, H., submitted for publication. Recognition and correlation of Mesoproterozoic Muva Supergroup rocks in the Neoproterozoic Lufilian and Zambezi belts of Zambia. Gondwana Research.

Tembo, F., De Waele, B., Nkemba, S., 2002. Syn- to post-orogenic granitoid magmatism in the Irumide belt of Zambia: geochemical evidence. African Geology Reviews 9, 1–17.

Theunissen, K., Klerkx, J., Melnikov, A., Mruma, A., 1996. Mechanisms of inheritance of rift faulting in the western branch of the East African Rift, Tanzania. Tectonics 15 (4), 776–790.

Thieme, J.G., Johnson, R.L., 1981. The geological map of Zambia (1:1.000.000). Geological Survey Department of Zambia, Lusaka.

Unrug, R., 1982. The Kasama Formation: lithostratigraphy, palaeogeography and regional position. In: Geological Society of Zambia, Palaeogeography of Zambia, Lusaka, pp. 2–8.

Unrug, R., 1984. The mid-Proterozoic Mporokoso Group of northern Zambia: stratigraphy, sedimentation and regional position. Precambrian Research 24, 99–121.

Van de Velde, P., De Waele, B., 1997. The geological map of the Mupamadzi River area. The Geological Survey Department of Zambia, Lusaka.

Van Tuijl, M.M., Verhoog, B.J., 1995. The geology of the Kalungu and Mututa Hills area; explanation of degree sheet 0932, SE and SW quarter. Report Geological Survey Department of Zambia 85.

Verhoog, B.J., Van Tuijl, M.M., 1995a. The geology of the Chozi area; explanation of degree sheet 0932, NW quarter. Report Geological Survey Department of Zambia 84.

Verhoog, B.J., Van Tuijl, M.M., 1995b. The geology of the Makasa area; explanation of degree sheet 931, SE quarter. Report Geological Survey Department of Zambia 86.

Verhoog, B.J., Van Tuijl, M.M., 1995c. The geology of the Nakonde area; explanation of degree sheet 0952 NE quarter. Report Geological Survey Department of Zambia 84.

Vrána, S., 1972. Some recently identified minerals new to Zambia. Records of the Geological Survey of Zambia 12, 91–94.

Vrána, S., Kachlík, V., Kröner, A., Marheine, D., Seifert, A.V., Ilášek, V., Babůnek, J., 2004. Ubendian basement and its late Mesoproterozoic and early Neoproterozoic structural and metamorphic overprint in northeastern Zambia. Journal of African Earth Sciences 38, 1–21.